

[Return to Index](#)

**MULTI-SEASONAL PREDICTABILITY AND CLIMATIC TRENDS FOR
SOUTH-WEST WESTERN AUSTRALIA**

B.G. Hunt, I.N. Smith, R.J. Allan and T.I. Elliott



CSIRO Atmospheric Research
PMB1 Aspendale, Vic 3195 Australia
Phone: (03) 9239 4680 Fax: (03) 9239 4688
E-mail: barrie.hunt@dar.csiro.au

**Phase 1 report to the
Indian Ocean Climate Initiative**

TABLE OF CONTENTS

TABLE OF FIGURES	56
THE CSIRO ATMOSPHERIC RESEARCH COMMITMENT TO THE INDIAN OCEAN CLIMATE INITIATIVE PROJECT	59
Objectives.....	59
Outcomes.....	59
SUMMARY	60
INTRODUCTION	62
PREDICTIONS AND SYNOPTIC FEATURES	63
(a) Rainfall prediction capabilities: globally, and for south-west Western Australia.....	63
(b) The Antarctic Circumpolar Wave and its influence over southern Australia.....	70
(c) Indian Ocean sea surface temperature anomalies and Western Australia rainfall.....	74
(d) Long-term observed global climatic trends.....	78
(f) Synoptic study.....	83
CONCLUDING REMARKS	120
FUTURE RESEARCH OPTIONS	121
Specific Projects.....	121
REFERENCES	123

TABLE OF FIGURES

Figure 1	Observations and predictions of the Southern Oscillation Index for 1971-1992, upper panel. Middle panel 10 member hindcast ensemble results. Bottom panel standard deviation of hindcast ensemble.....	65
Figure 2	Observations and predictions of rainfall for 1979-1991 for three island groups in the tropical Pacific Ocean. Each prediction begins on 1 January.	66
Figure 3	Observations and predictions of rainfall for 1979-1991 for a central Queensland region, upper panel. Middle panel rainfall anomalies. Bottom panel 10 member hindcast ensemble results.	68
Figure 4	Observations and predictions of rainfall for SWWA for 1979-1991. For the upper panel only two grid boxes were used in the area averaging, while nine grid boxes were used in the lower panel.	69
Figure 5	Regression pattern of observed SST upon observed 500 mb geopotential height. Results are shown for the first three EOFs of the SST.	72
Figure 6	Australian rainfall anomalies (mm/day) associated with SST EOF3 of the ACW at different lags.....	73
Figure 7	Correlation of a northwest wind index for July with July rainfall, upper panel and with August SST, bottom panel. Results from a 1000-year simulation.....	76
Figure 8	Zonal (upper panel) and meridional (low panel) low-level wind velocity anomalies from the HINDCAST run. The black areas are regions where mountains exclude the low-level wind.....	77
Figure 9	EOF1 time series of combined near global distributions of sea surface temperature and mean sea-level pressure, band-passed filtered for the periods 11-13 years, 15-20 years and 20-30 years.....	79
Figure 10	EOF2 of combined near global distributions of sea surface temperature and mean sea-level pressure, band-passed filtered for periods greater than 39 years. The upper panels show the spatial patterns and the lower panel shows the associated time series.	80
Figure 11	Spatial distributions of the correlations between MSLP and SST and SWWA JJA rainfall are shown in the left and right hand panels respectively. The top panels are for JJA conditions, the middle panels for MAM and the bottom panels for May alone conditions. The correlations are based on observations for the period 1950-1994.....	82
Figure 12	Observed and fitted SWWA JJA rainfall anomalies for the period 1950-1994. The fitted results were obtained by computing regressions between May MSLP and SST for 10° by 10° boxes centred over regions of maximum correlation for May in Figure 11, and then using the regressions to compute the results shown in the figure. The top panel is for MSLP and the bottom panel for SST.....	84
Figure 13	Sequence of 24-hour rainfall totals (mm) over the period 22-25 July 1996 according to NCEP/NCAR reanalysis data. 22 July (<i>upper left panel</i>), 23 July (<i>upper right panel</i>), 24 July (<i>lower left panel</i>) and 25 July (<i>lower right panel</i>). The black shading encloses values greater than 6 mm.....	86
Figure 14	Five-day sequences of rainfall over Australia simulated with the CSIRO Mark 2 model forced with the observed GISST data set. Results are shown for four separate simulations, which differed only in the initial conditions used in 1871. Each individual page of the figure shows five consecutive days starting on 28 June 1991. The darker shading in the figure corresponds to heavier rainfall. In each panel the underlying surface pressure distribution is shown. <i>Simulation number 1</i>	87
Figure 14	Continued. <i>Simulation number 2</i>	88

Figure 14	Continued. <i>Simulation number 3</i>	89
Figure 14	Continued. <i>Simulation number 4</i>	90
Figure 15	A six-day sequence of rainfall for the Australian region in January from the CSIRO Mark 3 model. The rainfall is associated with a ‘tropical cyclone’ type system. The rainfall is shown in mm/day.	92
Figure 16	The sea-level pressure distributions corresponding to the rainfall sequence shown in Figure 15. The surface pressures are in mb.	93
Figure 17	Locations where rainfall trends of a given duration were found at least once in the 1000-year simulation are identified by black rectangles. The upper panels show negative and positive trends of 10-years duration in the left and right hand panels respectively. The lower panels repeat this information for trends of 12-years duration.	96
Figure 18	Locations where screen temperature trends of 15 years duration were found at least once in the 1000-year simulation are identified by black rectangles. The upper panel shows results for negative 15-year trends, the lower panel for positive 15-year trends.	97
Figure 19	Locations where multiple rainfall trends of 10-years duration were found in the 1000-year simulation are identified by rectangles. Results for negative 10-year trends are shown in the upper panel, for positive 10-year trends in the lower panel. A rectangle identified with, say, 3, indicates that there were three 10-year periods found in the 1000-year simulation, implying a return period of 333 years.	100
Figure 20	As for Figure 19, only for 15 year screen temperature trends.	101
Figure 21	Locations where screen temperature, rainfall and surface wind stress with 10-year negative trends occurred in the timeframe 60-625 years of the 1000-year simulation are shown by black rectangles.	102
Figure 22	Locations where negative 10-year trends of screen temperature occurred in three separate 25 year periods are shown by black triangles. The individual periods are identified on each panel.	103
Figure 23	The percentage rain loss per year for negative and positive 10-year rainfall trends are shown in the upper and lower panels respectively.....	104
Figure 24	Cumulative rainfall anomalies for three model grid boxes, identified by longitude and latitude in the individual panels, from the 1000-year simulation.....	105
Figure 25	Histograms of annual rainfall anomalies from the 1000-year simulation for a model grid box in the central Pacific Ocean.....	107
Figure 26	Histograms of annual rainfall anomalies from the 1000-year simulation for a model grid box in SWWA.....	107
Figure 27	Histograms of annual mean screen temperature anomalies from the 1000-year simulation for the same model grid box in SWWA as used in Figure 26.....	109
Figure 28	Histograms of annual mean screen temperature anomalies from the 1000-year simulation for a model grid box in the south Pacific Ocean, 220°E, 40°S.....	109
Figure 29	Histograms of screen temperature anomalies from the 1000-year simulation for a model grid box in the Southern Ocean, 130°E, 55.7°S.....	110
Figure 30	Observed sea surface temperature anomalies from the GISST data set. Results for the northwest Pacific Ocean (170°E, 45°N) are shown in the upper panel, and for the south central Pacific Ocean (220°E, 40°S) in the lower panel.....	113
Figure 31	Oceanic temperature anomalies at various depths for a given year of the 1000-year simulation. The colour code identifier under the various plots is in °K.....	114

Figure 32	Histograms of screen temperature and ocean temperature anomalies from the 1000-year simulation for the same model grid box as used in Figure 28 (i.e. South Pacific Ocean, 220°E, 40°S).	115
Figure 33	A sequence of rainfall anomalies from the 1000-year simulation associated with an eight-year drying trend in SWWA.....	116
Figure 34	One-point correlation map for SWWA for screen temperature from the 1000-year simulation.	118
Figure 35	Simulated annual mean rainfall changes over SWWA under greenhouse conditions. The effective CO ₂ content of the atmosphere was tripled between 1881 and 2083 AD and held constant thereafter. The thin line represents annual mean values for individual years, the thick line is a time-smoothed version of that curve.....	119

THE CSIRO ATMOSPHERIC RESEARCH COMMITMENT TO THE INDIAN OCEAN CLIMATE INITIATIVE PROJECT

The following are the agreed objectives for CSIRO Atmospheric Research under Phase 1 of the Indian Ocean Climate Initiative Project contract:

Objectives

- assess and compare rainfall prediction capabilities both globally and locally over south-west Western Australia;
- evaluate wind stress over the oceans, particularly the Indian Ocean. Wind stress may be one of the main mechanisms linking SST forcing from the Pacific with the Indian Ocean and hence south-west Western Australia climate;
- examine the synoptic situations under which rainfall occurs in south-west Western Australia and endeavour to relate to south-west Western Australia patterns within the model;
- assess limits of predictability;
- identify long-term dry/rain trends on a global basis. Highlight spatial patterns involving significant trends in south-west Western Australia;
- search for mechanisms underlying trends.

Outcomes

- ability to identify climate mechanisms and relationships;
- climate model data sets as input to statistical forecasting and downscaling studies;
- baseline of current mechanistic forecasting capability for south-west Western Australia;
- estimates of long-term rainfall variability for south-west Western Australia;
- interim workshop report and contribution to consolidated report;

SUMMARY

Research has been completed on the objectives agreed to in this first phase of the Indian Ocean Climate Initiative Project.

The research was primarily related to the use of global climatic model outputs, and involved two separate components.

The first component was concerned with the ability of the model to replicate important features of the observed climate over south-west Western Australia, and to investigate multi-seasonal prediction capabilities for this region. The observed synoptic characteristics associated with rainfall were well simulated by the model. Sea surface temperature anomalies restricted to the low latitude Pacific Ocean are able to generate widespread surface wind anomalies, those over the Indian Ocean being particularly relevant to Western Australia. Results from a 1000-year climatic simulation suggest that wind systems associated with the Indian Ocean are responsible for both the observed sea surface temperature anomalies in the Indian Ocean *and* rainfall perturbations over Australia.

Predictions of rainfall over south-west Western Australia using a global climatic model were found to be of limited skill and lacked the observed interannual variability. The Antarctic Circumpolar Wave has a potentially significant impact on this region, and the poor representation (if at all) of this phenomenon in the predictions may have contributed to the low skill.

An analysis of observational data indicated that there is potential predictability for winter rainfall over south-west Western Australia associated with mean sea level pressure and sea surface temperatures in May to the west and south of Australia.

While this preliminary search has indicated that multi-seasonal predictions for south-west Western Australia have a number of problems to be resolved, the advent of the CSIRO Mark 3 model should considerably improve our ability to simulate the climate of this region.

The second component of this research project involved the use of outputs from a 1000-year simulation using the CSIRO Mark 2 coupled climatic model. Analysis of climatic trends revealed that rainfall trends greater than about 10 years duration were an exceptional feature of climatic variability (depending upon how such trends are defined). Temperature trends

were found to be typically of longer duration, such trends being reasonably common over much of the globe. The return period of a 10-year rainfall trend was found to be of the order of 1000 years; only a few locations had two or more such trends in the 1000 years of the simulation. Drying trends were principally identified with arid regions, indicating underlying mechanistic influences. Annual rainfall losses of 20-30 per cent were found to be associated with such drying trends.

Time series of climatic anomalies in the 1000-year simulation, displayed as histograms, permitted trends and other temporal variations to be readily identified. The results suggest that the present drying trend over south-west Western Australia is not unique. An examination of the synoptic rainfall distributions associated with an eight-year drying trend in this region revealed that a single, dominant synoptic characteristic did not occur. Thus a single mechanistic process probably does not exist.

Given the important role of sea surface temperature anomalies in initiating climatic perturbations, an extensive analysis of such anomalies was made. Decadal and multi-decadal cooling and warming trends were readily identified in the model, and it was possible to associate these with oceanic temperature anomalies which extend below the surface to depths of 100 meters or so. How such persistent anomalies induced climatic teleconnection and perturbations in the model is unclear.

Finally, a study was made of the spatial characteristics associated with the climate of south-west Western Australia. It was found that this region is relatively isolated climatologically; in particular, teleconnection to the climatic 'heat engine' of the low-latitude Pacific Ocean was not established.

INTRODUCTION

South-west Western Australia (SWWA) is currently facing a number of climatically-related problems. The most critical is the drying trend that has persisted since about 1970. Superimposed upon this *climatic variability* problem is the possibility of future greenhouse-induced *climatic change*. Both of these are long-term issues. A separate, short-term issue is the need to be able to predict rainfall two or more seasons in advance to enable planning over the critical summer period.

Long-term (multi-decadal) climatic trends are a relatively poorly understood climatological feature. Some trends are particularly well-publicised, such as the dust bowl in the mid-west USA in the 1930s, and the severe drought in the Sahel commencing in 1968. Others, such as the anomalous wet trend in the Flinders Ranges of South Australia in the 1880s are documented largely by abandoned settlements. There has been little research into the causes of these trends.

Greenhouse-induced climatic change has the potential to create regional climatic anomalies or trends of relevance to SWWA. Earlier research by CSIRO Atmospheric Research has been documented in a number of reports, such as Suppiah *et al.*, 1998. No study of the greenhouse effect specific to SWWA has, however, been commissioned.

Much progress has been made in the past decade in the development of global climatic models for multi-seasonal predictions. Such prediction schemes involve the use of coupled oceanic-atmospheric models (Palmer and Anderson, 1994). The major precursor for the predictions are El Niño-Southern Oscillation (ENSO) events. Currently, the level of skill involved in these models is not particularly high, although the ability to predict sea surface temperature (SST) anomalies associated with a given ENSO event is improving to the extent that the more comprehensive dynamical models now appear to perform better than the simpler models (Barnston *et al.*, 1999). Useful predictions of rainfall are notoriously difficult to make (see Stockdale *et al.*, 1998). There have been a number of studies of the *predictability* of the climatic system (e.g. Rowell, 1998) that attempt to identify regions where predictive skill is expected to be useful and these indicate that modest skill for rainfall is possible over SWWA.

A problem that compounds development of prediction skill is the occurrence of secular variability. Analysis of lengthy observational time series reveals that a number of cycles of varying duration, from the quasi-biennial to multi-decadal, exist (Allan, 1999). The interactions between such cycles can greatly alter the success of a multi-seasonal prediction.

This report indicates the nature of the problems that need to be addressed within the Indian Ocean Climate Initiative Project. These problems are complex, interactive, nonlinear and of multi-timescales and will not be easy to resolve.

PREDICTIONS AND SYNOPTIC FEATURES

(a) Rainfall prediction capabilities: globally, and for south-west Western Australia

Multi-seasonal climatic predictions are based on a prior knowledge of SST distributions, with global distributions being preferred. These SST distributions can then be used to ‘force’ an atmospheric global climate model to provide a prediction.

The major component of this phase of the project was to use existing hindcasts (i.e. retrospective predictions) to assess multi-seasonal prediction capabilities over SWWA. Two rather different approaches are reported. The first involves using SSTs for the low latitude Pacific Ocean only, hindcast by a US group for 1971-1991. These hindcast SSTs were combined with climatological SSTs for the rest of the oceans to force a T63 ($1.875^\circ \times 1.875^\circ$) horizontal resolution version of the CSIRO Mark 2 atmospheric global climate model. The second approach uses observed global SSTs for the same period to ‘force’ the same global climate model. In effect, the latter approach represents the ‘ultimate’ prediction in that the best available SST data set is used. This is the GISST (Global sea-Ice and Sea Surface Temperature) data set. All results associated with it are identified as “GISST” in this report. The results from the low latitude Pacific Ocean case will be identified as “HINDCAST”. For convenience, outputs from these two runs will be subsequently referred to as predictions. See Hunt (1999b) for more details.

Because of chaos in the climatic system, multiple runs or ensembles were necessary for both prediction cases. Ten-member ensembles were made for the HINDCAST and four-member ensembles for the GISST runs. Ensemble mean results will generally be presented here.

Results for a number of regions as well as SWWA will be presented to illustrate the potential that exists for such predictions.

The primary cause of interannual climatic variability over Australia is El Niño – Southern Oscillation (ENSO) events, hence the skill of any prediction scheme will ultimately be determined by how well these events are predicted. The Southern Oscillation Index (SOI) represents a recognised criterion used to determine the status of ENSO events and is also used in statistical methods to predict rainfall (Stone *et al.*, 1996); hence just the prediction of this index is of interest.

Figure 1(a) compares observed, HINDCAST and GISST time series of the Southern Oscillation Index for the period 1971-1991, which embraces a number of major events. Each prediction is for a 12-month period commencing on 1 January, and the time series in Figure 1 are broken at the end of each year to define the duration of the predictions. Three major El Niño events occurred during this period, and each one was captured in the predictions. While there are differences between the high frequency details of the three time series, the most critical feature – the transition between ENSO states – is captured particularly well by the model. As would be expected, the GISST values are more skilful than the HINDCAST, although there are some discrepancies, such as in 1980 and 1987.

The 10 individual runs of the HINDCAST are shown in Figure 1(b) to illustrate the impact of chaos on a climatic feature such as the SOI. While the basic characteristics of the SOI time series are apparent, SOI values varying by 20 occur at any one time between the ten individual runs. This demonstrates the necessity of doing multiple runs in order to obtain a representative mean.

The standard deviation of the HINDCAST SOI ensemble is given in Figure 1(c). The largest deviations are associated with peak negative SOI values for El Niño events when the forcing SST anomalies reach their largest amplitudes.

Figure 2 compares HINDCAST and GISST rainfall results with observations at three locations in the tropical Pacific where the highest skill occurs. Each time series shown represents the results for a *single* model grid box ($1.875^\circ \times 1.875^\circ$) and represents the finest spatial detail possible with this model. Overall, the interannual variability – usually the most important feature in any prediction – is well captured by the predictions. The highest skill was obtained for the Phoenix Islands, Figure 2(b), where the SST values reached their maximum during El Niño events.

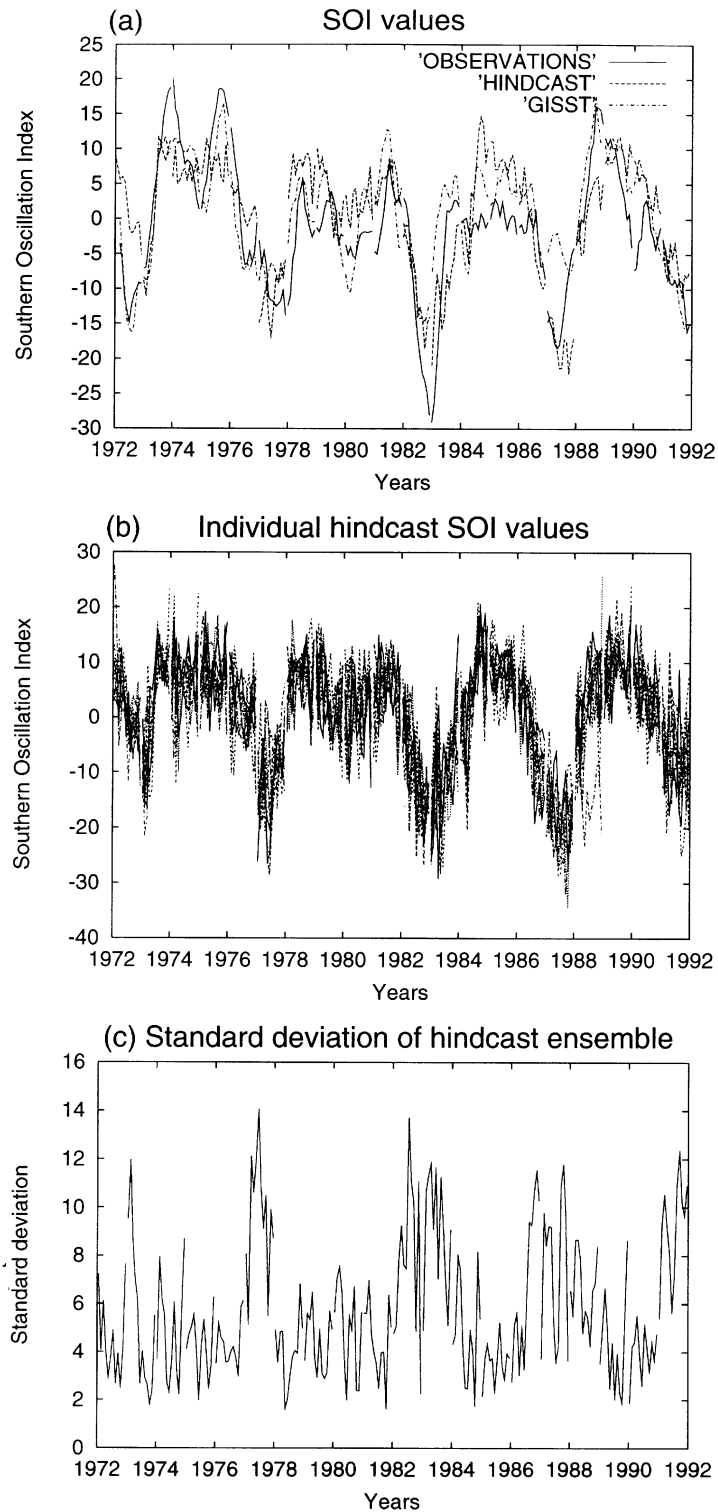


Figure 1 Observations and predictions of the Southern Oscillation Index for 1971-1992, upper panel. Middle panel 10 member hindcast ensemble results. Bottom panel standard deviation of hindcast ensemble.

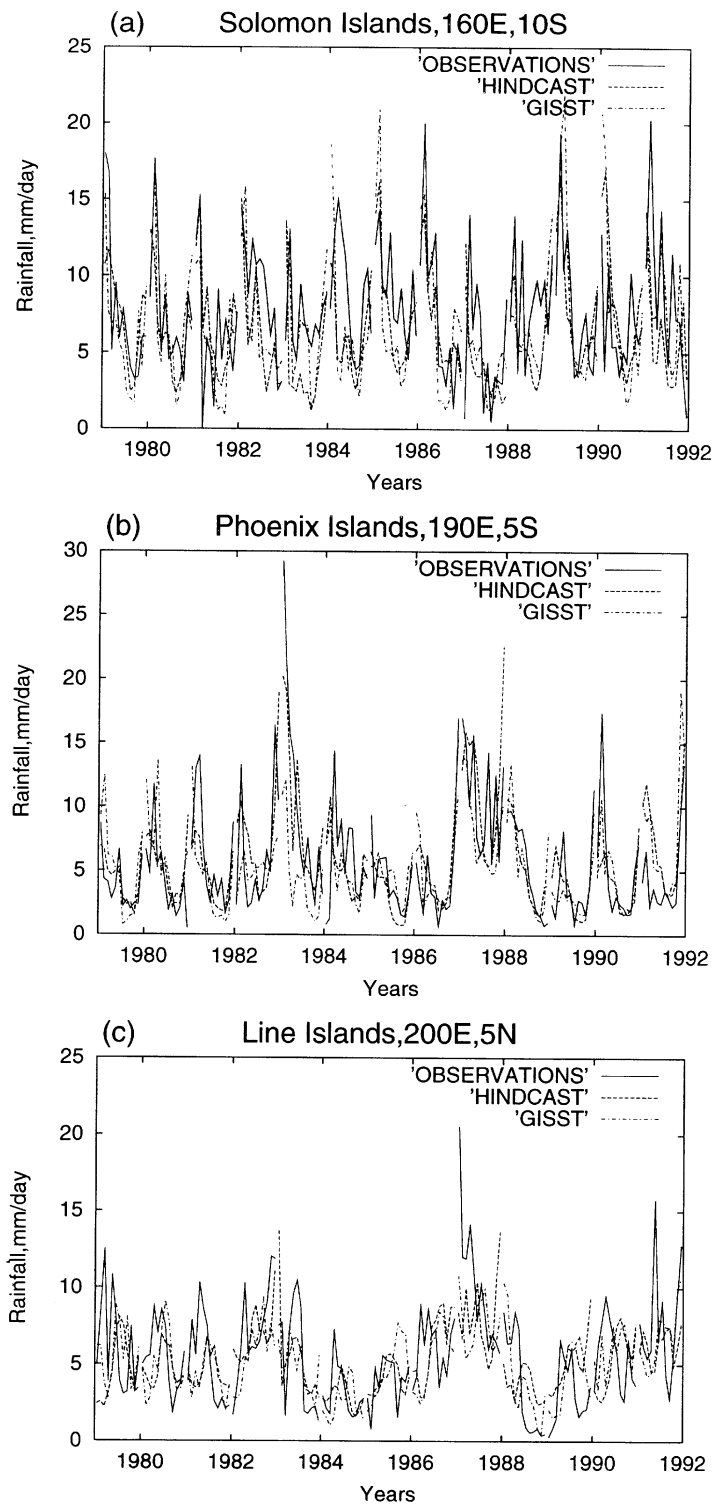


Figure 2 Observations and predictions of rainfall for 1979-1991 for three island groups in the tropical Pacific Ocean. Each prediction begins on 1 January.

Away from the tropical Pacific, predictive skill deteriorates as the impact of the ENSO events declines. It then becomes necessary to use spatial averaging over several grid boxes to obtain a representative signal. Figure 3(a) shows time series of rainfall for observations and predictions for a region in central Queensland representing approximately 20 per cent of that state.

In this example, the GISST results are not encouraging. The HINDCAST results reproduce much of the observed interannual variability — note, in particular, the drought years of 1982 and 1987 and the enhanced rainfall in the following years. In the 1990s, the HINDCAST values were poor because the predictions of SST anomalies for the low latitude Pacific Ocean essentially failed. The rainfall anomalies for this region shown in Figure 3(b) exhibit more variability, but the model captured the strong ENSO events such as that in 1982. Closer inspection reveals that considerable temporal disagreement exists between the results in any one year. This raises the question of whether a temporal resolution of one month, as used in this figure, is viable in practice or should only seasonal means be presented.

Finally, in Figure 3(c), the 10 values generated from the HINDCAST runs are reproduced to illustrate the range of variability in rainfall owing to chaotic effects. The variability across the 10-member ensemble for a given month is large and reinforces the need to use multi-member ensembles in predictions.

Figure 4 shows rainfall predictions for two regions encompassing SWWA. In Figure 4(a), only two model grid boxes were used in the analysis, while for Figure 4(b), nine grid boxes were selected. The sensitivity of the results to area averaging is quite apparent. Fair agreement is obtained between the two model outputs in both examples, suggesting that the major forcing in the model derives from the low latitude Pacific Ocean. Somewhat better agreement is obtained between the two model runs and observation for the larger region, Figure 4(b), although there is a bias towards over-estimation of rainfall in the model. This is in contrast to the smaller region used in Figure 4(a), where the model systematically underestimated the observed rainfall.

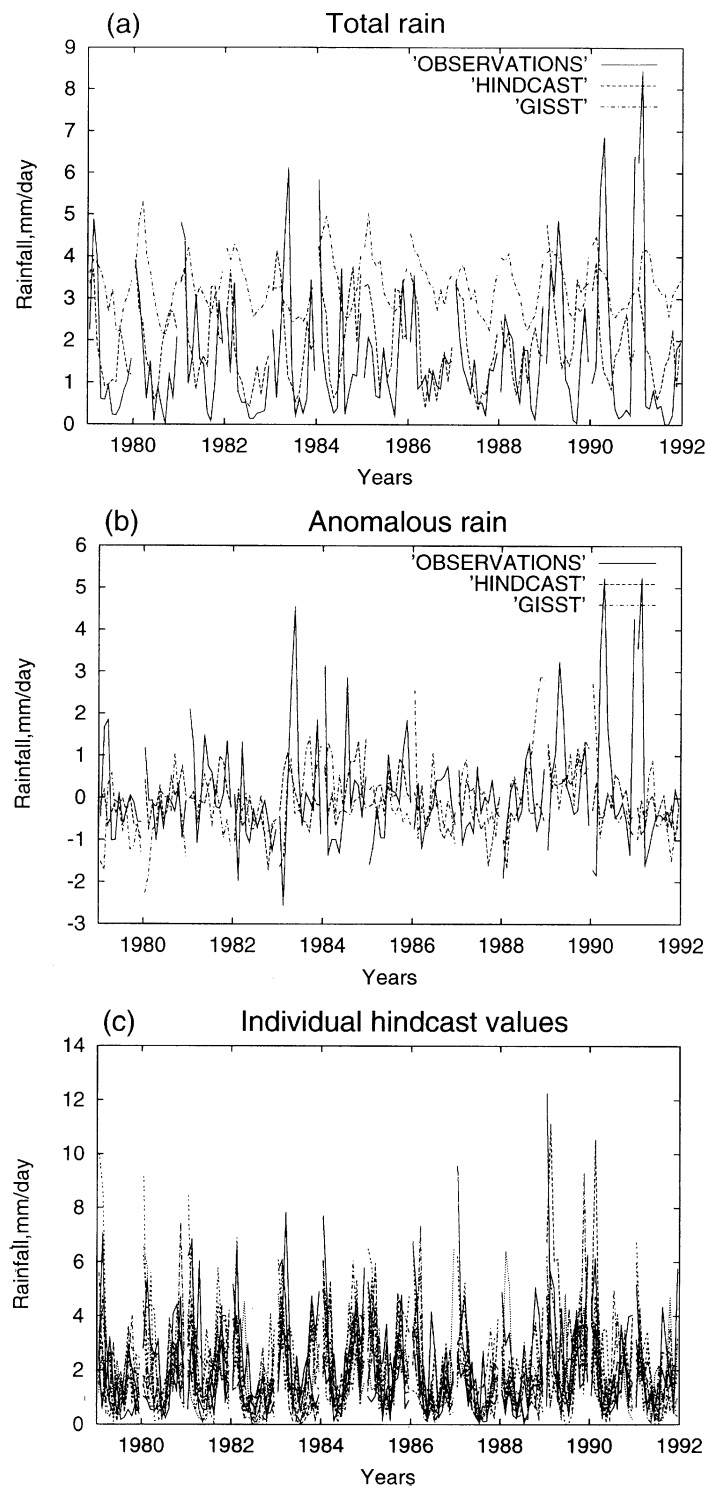


Figure 3 Observations and predictions of rainfall for 1979-1991 for a central Queensland region, upper panel. Middle panel rainfall anomalies. Bottom panel 10 member hindcast ensemble results.

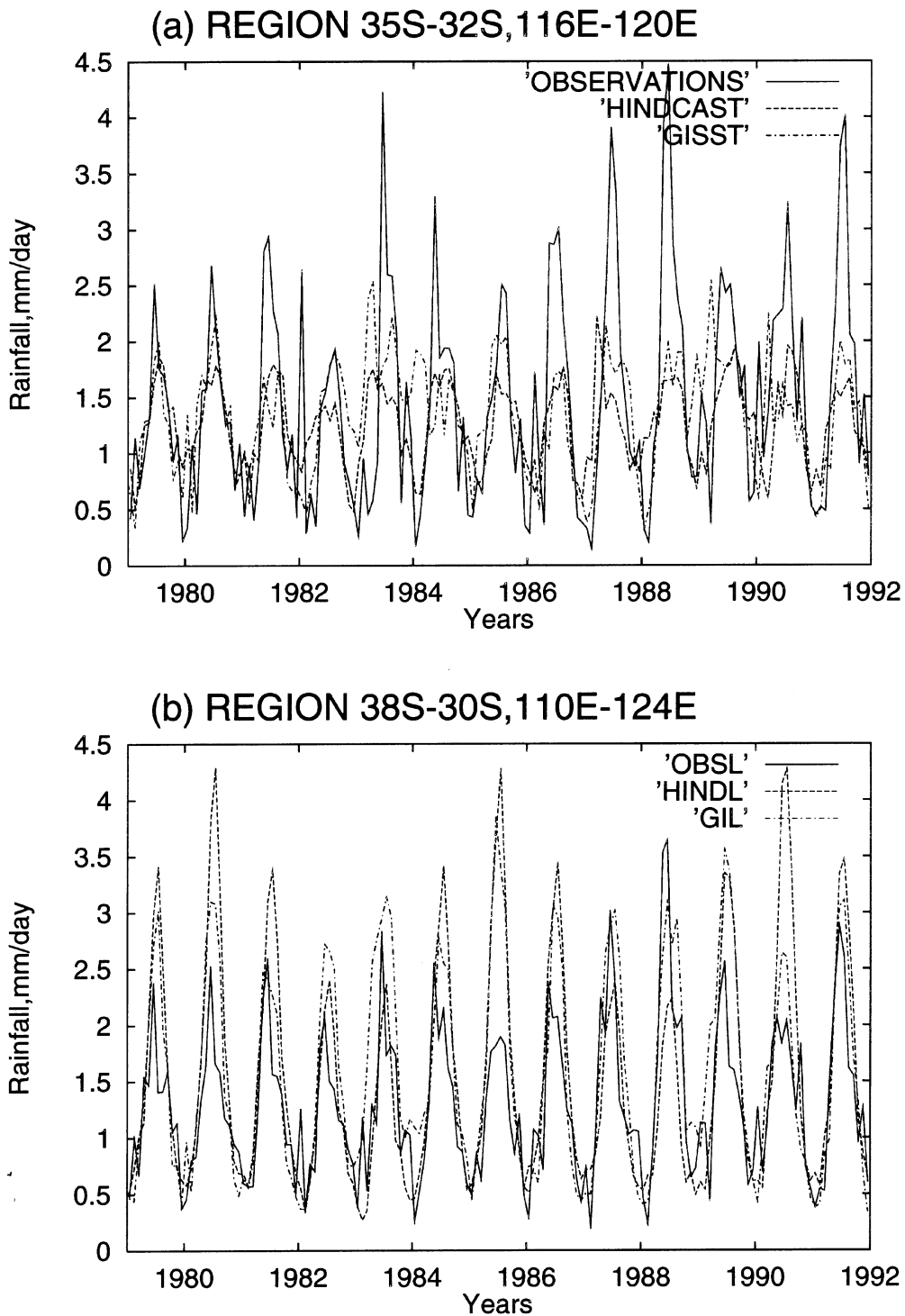


Figure 4 Observations and predictions of rainfall for SWWA for 1979-1991. For the upper panel only two grid boxes were used in the area averaging, while nine grid boxes were used in the lower panel.

In general, the model failed to capture the observed interannual variability, suggesting that a *direct* influence of low latitude Pacific Ocean SST is not a major precursor for SWWA rainfall. The GISST results appear closer to the observations indicating that the SSTs elsewhere (possibly the Indian Ocean) may have an influence on SWWA rainfall. It should be noted that the GISST model results may suffer from poorly observed high southern latitude SST values where data are relatively sparse. A detailed analysis would be required to determine the various causes contributing to the poor model interannual variability. Certainly, with an improved model and a better SST data set it should be possible to improve predictability in SWWA. This is an option which can be explored in future research.

(b) The Antarctic Circumpolar Wave and its influence over southern Australia

The Antarctic Circumpolar Wave (ACW) is a long-lived (order of decadal) phenomenon involving anomalies in SSTs, mean sea level pressure, winds and sea ice in high southern latitudes. Recent analysis at CSIRO Atmospheric Research, unrelated to the Indian Ocean Climate Initiative Project, has highlighted the potential influence of the ACW on southern Australia. This influence could be relevant to both multi-seasonal predictions as well as the long-term rainfall deficit in SWWA. In this report, we present a simple documentation of some observations.

SST anomalies associated with the ACW were generated by band pass filtering observed SSTs and retaining outputs for a 3-7 year period. Results were then subjected to an Empirical Orthogonal Function (EOF) analysis with the first three modes being retained; these modes account for 75% of the total variance. In order to obtain spatial patterns representative of the ACW, the temporal coefficients of the three EOFs were regressed against observed (NCEP/NCAR reanalysis) 500 hPa geopotential heights. Figure 5 shows the three regression patterns. The first mode is attributed to El Niño – Southern Oscillation events and is dominated by a wave number 2 pattern at high latitudes. The second mode has a wave number 3 pattern and is readily produced in the CSIRO global climate model. The third mode displays a wave number 2 pattern, but its origin is less clear. Since all three modes contribute to the observed ACW SST anomalies, it can be appreciated that complex interactions can occur which may influence southern Australia's climate.

These modes can have marked impacts on Australian rainfall variability. Rainfall anomalies associated with the individual ACW EOFs of SST were obtained by regressing observed

rainfall upon the SST EOF time series, at different lags, and then scaling the results at each grid box to correspond with one standard deviation of the EOF time series. Figure 6 shows such rainfall anomalies for EOF3, which had the largest response. For a given lag, a positive anomaly at a particular location implies that rainfall increases in phase with the EOF time series. The figure reveals a strong eastward propagating signal as SST anomalies are advected eastwards. Importantly, in Western Australia and the southern states the influence of EOF3 is greater than that of the El Niño – Southern Oscillation EOF1 mode of the ACW. See Cai *et al.* (1999) for further details.

Although the absolute magnitude of the rainfall anomalies in Figure 6 (scaled to one standard deviation) is small ($\sim 0.2 \text{ mm day}^{-1}$), the cumulative influence over a year would be substantial. Hence, the influence of the ACW needs to be included in future studies of Western Australia.

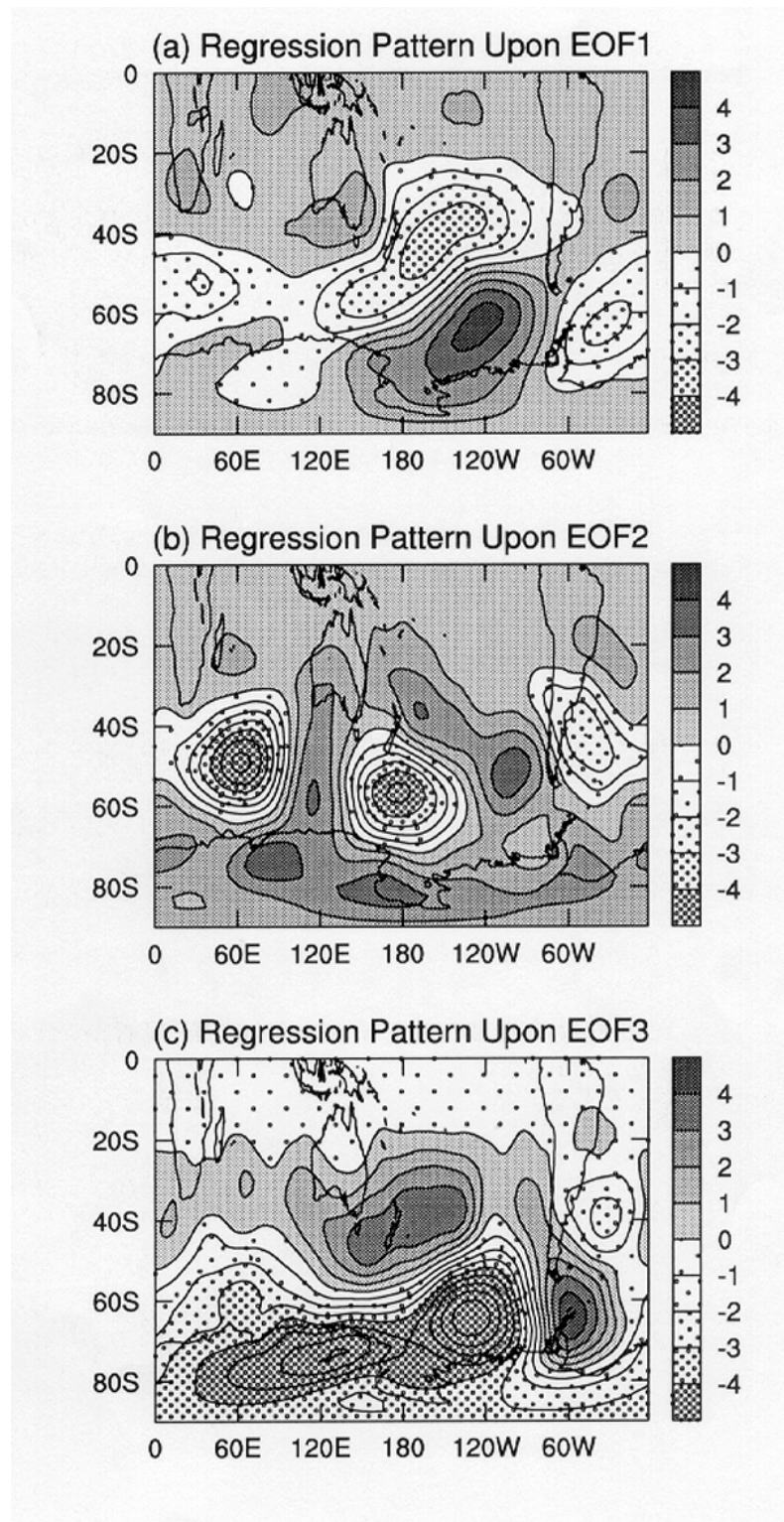


Figure 5 Regression pattern of observed SST upon observed 500 mb geopotential height. Results are shown for the first three EOFs of the SST.

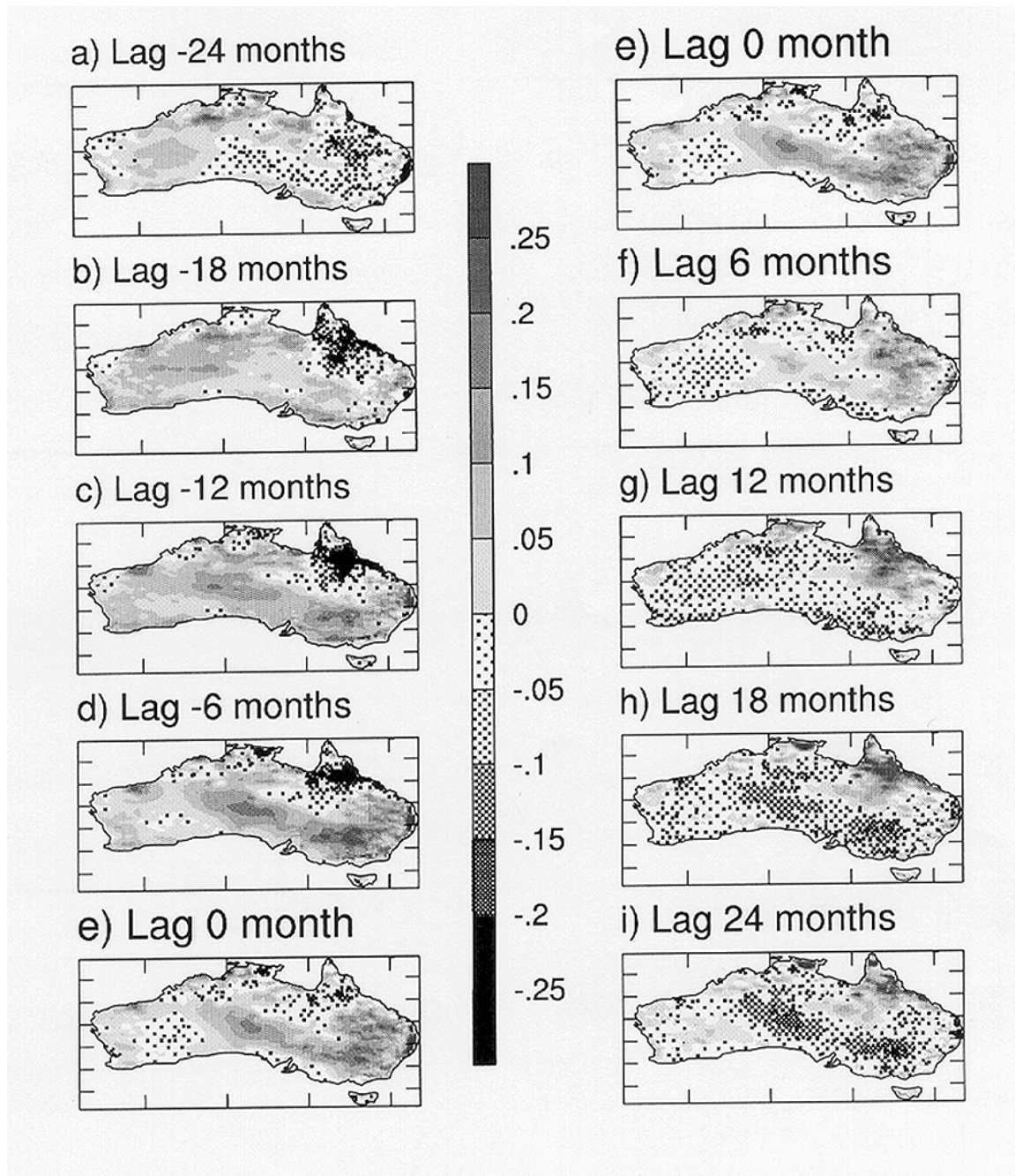


Figure 6 Australian rainfall anomalies (mm/day) associated with SST EOF3 of the ACW at different lags

(c) Indian Ocean sea surface temperature anomalies and Western Australia rainfall

In an analysis unrelated to the Indian Ocean Climate Initiative Project, Dr Ian Watterson of CSIRO Atmospheric Research has analysed results from a 1000-year run of the CSIRO Mark 2 coupled model to examine relationships between Indian Ocean SST anomalies and rainfall over Australia. There have been numerous studies of such relationships (see for example Smith *et al.*, 1999), which suggest that SST anomalies in the Indian Ocean are the precursor to rainfall perturbations extending from the north-west to the south-east over Australia. In particular, Nicholls (1989) identified a SST anomaly dipole in the Indian Ocean, with warm anomalies around northern Australia and cool anomalies over the central Indian Ocean, which he found correlated well (~ 0.6) with winter rainfall over much of Australia. However, Simmonds and Trigg (1988), in simulations with a global climatic model using specified SST anomalies, were unable to capture such specific features.

The SST anomalies in the 1000-year simulation used by Watterson were freely evolving as part of the natural climatic variability existing in such a coupled model. The analysis conducted was rather complicated, but was designed to isolate the contribution of the north-west component (from EOF analysis) of the July 800 hPa wind over Australia to winter rainfall and SST variability in the Australian region. Effectively, the upper panel of Figure 7 shows the percentage variance explained when a wind index based on the north-west July 800 hPa wind is correlated with July rainfall, while the lower panel shows how much the wind index explains August surface temperature. The latter is for the time of the peak correlation. Both panels in Fig 7 are similar to the observational results of Nicholls (1989), which serves as a validation of the model. The essential outcome is that while rainfall and northwest wind are coincident, the SST anomalies lag the rainfall. This indicates that the SST anomalies do not cause the rainfall anomalies, both appear to be forced by the northwest component of the wind.

Further analysis relating SST anomalies to rainfall predictions over Australia indicated that there was negligible predictability of winter rainfall from a May SST dipole pattern.

Clearly, north-west winds in winter over the Indian Ocean can have a major impact over large areas of Australia, including SWWA. Thus, the skill in predicting winter rainfall may be constrained by our ability to predict the underlying wind anomalies over the Indian Ocean. So, it is important to identify the sources of such wind anomalies. An important source in

this regard are SST anomalies in the low latitude Pacific Ocean associated with El Niño – Southern Oscillation events. The unique impact of such SST anomalies can be demonstrated by using output from the HINDCAST prediction runs referred to above. Figure 8 illustrates the global distribution of zonal and meridional low-level wind anomalies for September 1976 from the ensemble mean of the HINDCAST run, attributable essentially to low latitude Pacific SST anomalies used in those predictions. Wind anomalies of about $1-2 \text{ ms}^{-1}$ are generated by these anomalies. These are then able to produce associated rainfall and Indian Ocean SST anomalies. This result emphasises the need for skilful prediction of Pacific Ocean SST anomalies, along with a model's ability to generate appropriate wind anomalies, if Western Australian rainfall is to be predicted.

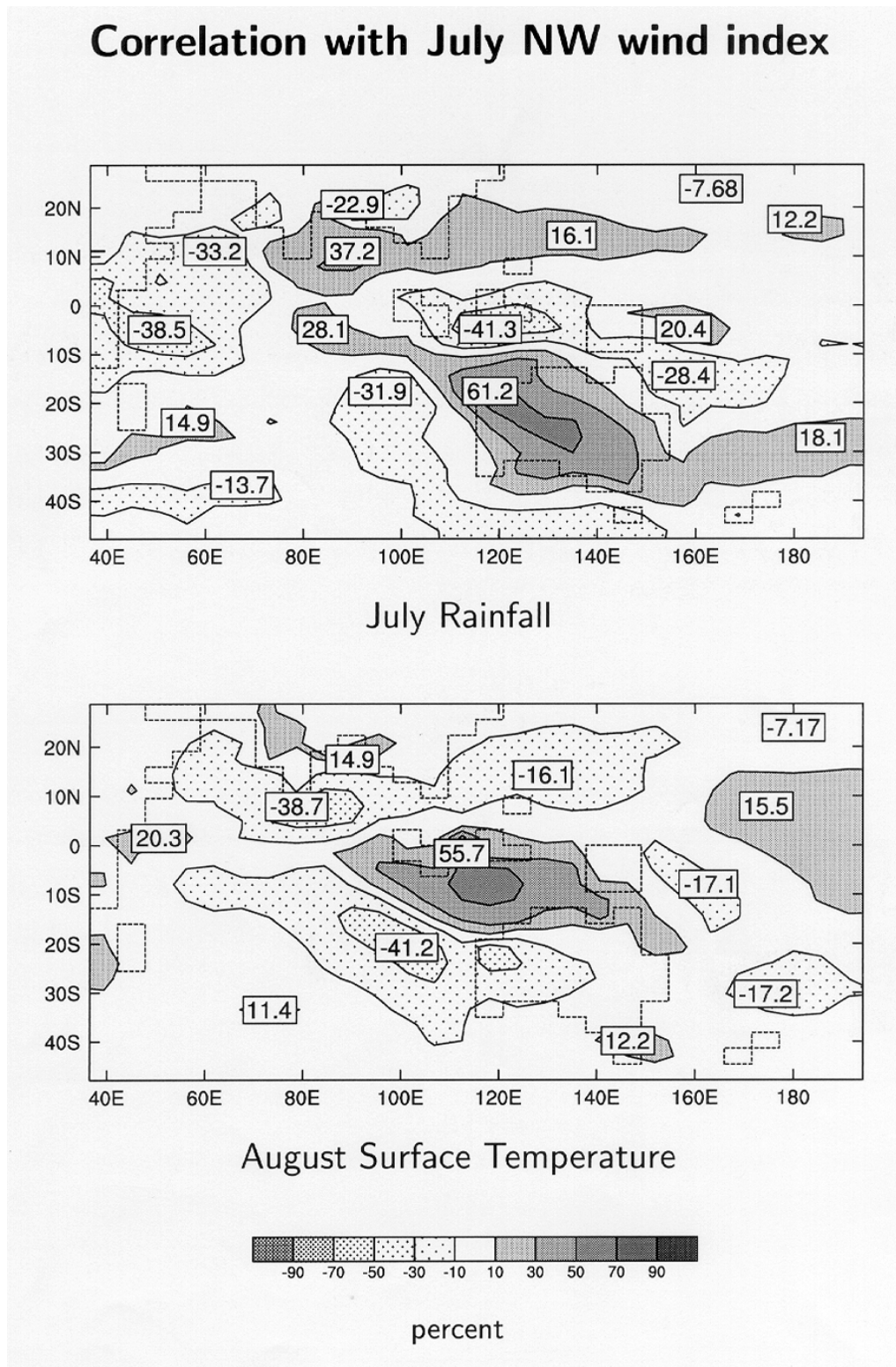
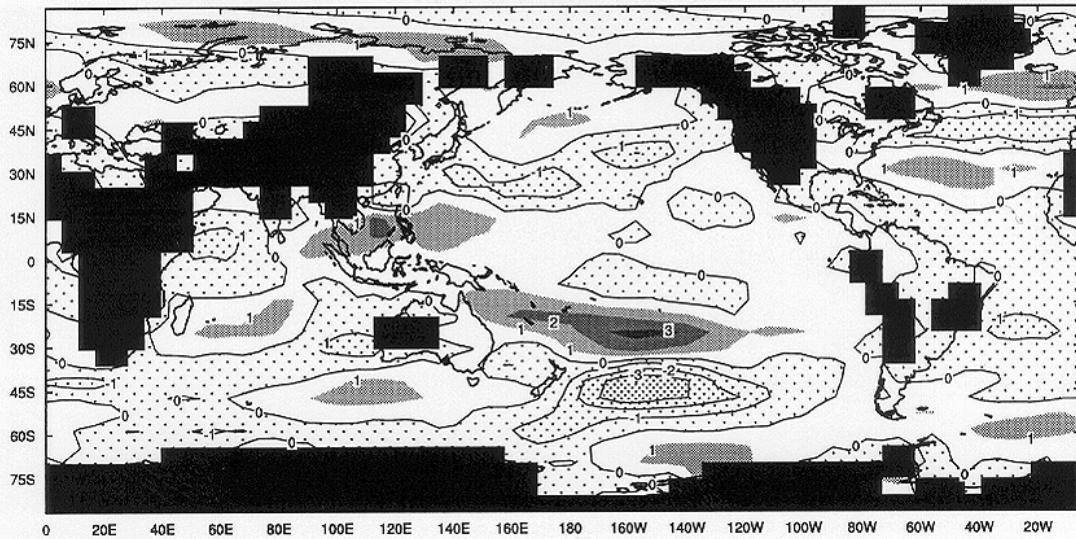


Figure 7 Correlation of a northwest wind index for July with July rainfall, upper panel and with August SST, bottom panel. Results from a 1000-year simulation

(a) Zonal velocity anomalies for September, 1976



(b) Meridional velocity anomalies for September, 1976

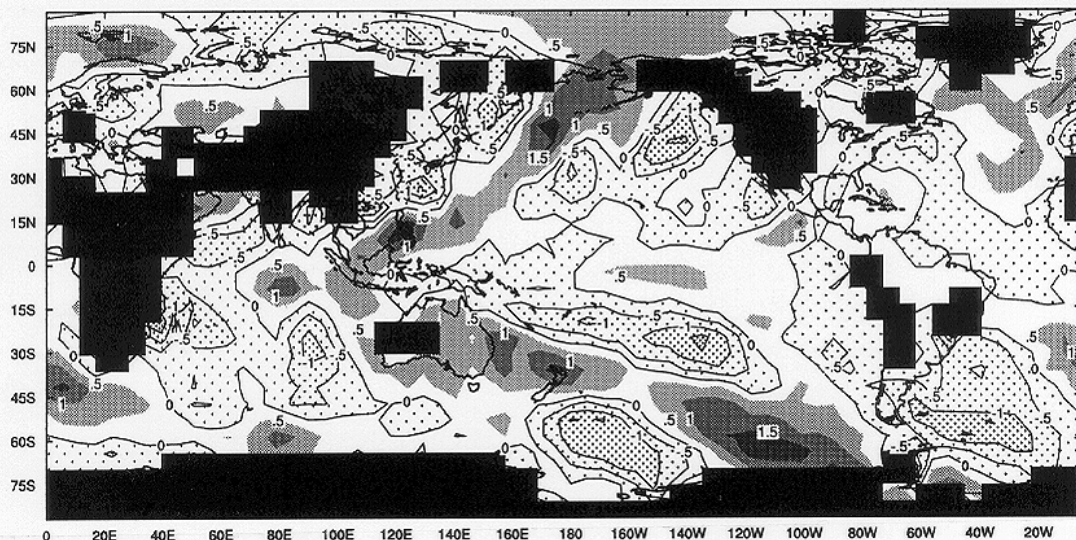


Figure 8 Zonal (upper panel) and meridional (low panel) low-level wind velocity anomalies from the HINDCAST run. The black areas are regions where mountains exclude the low-level wind.

(d) Long-term observed global climatic trends

In the 1990s, multiple and protracted El Nino episodes occurred. These caused major problems with the existing embryonic multi-seasonal prediction schemes. Such events are not unique, having occurred previously in the 1940s, 1910s and 1890s. Hence, it is important to understand the causes of such multiple events, as well as to ensure that they are included in predictions made with global climate models.

Analysis of observations (Allan, 1999) has revealed that there are a number of naturally-occurring periodicities in the climatic systems and that these periodicities can interact with one another, constructively or destructively, to influence the magnitude of a given climatic anomaly.

In Figure 9, band-pass filtered combined SST and sea-level pressure global data sets are shown for three selected periods as time series for EOF1. This illustrates how such periodicities are able to interact with one another.

The spatial patterns associated with the EOFs of a given periodicity are illustrated in Figure 10. This figure shows EOF2 for periods longer than 39 years. Large-scale patterns are evident, with a ENSO-type signal apparent *for this particular EOF* in both the sea-level pressure and the SST signals in the Pacific Ocean.

In order to capture such effects in models, it will be necessary to initialise the oceanic component of the model, where the long-term memory of the climatic system resides, with appropriate forcing agents.

Thus, these long-term periodicities and the role of the Antarctic Circumpolar Wave highlight the need to incorporate the ocean's evolution into the data sets to be used in multi-seasonal predictions.

(e) **Predictability assessment for south-west Western Australia**

Table 1 presents correlations between observed SWWA winter rainfall and the mean sea level pressure (MSLP) for Perth, Darwin and Tahiti, together with corresponding correlations for the SOI. Results are given for two periods, 1907-1994 and 1950-1994. The correlations are stable over these two periods, in spite of improvements in the observational data base in the latter period. The correlations show that June, July and August (JJA) rainfall alone has a useful correlation with the simultaneous mean sea level pressure at Perth. The mean sea level pressure at Perth for May or March, April and May (MAM) provides no predictive indication for SWWA JJA rainfall. The high negative correlation of -0.8 in JJA in Table 1 for Perth mean sea level pressure implies that SWWA rainfall is associated with cyclonic, or low surface pressure, conditions. The modest (0.3) correlation with the SOI in Table 1 helps to explain the limited skill shown in Figure 4 for the predictions, as the SOI is strongly influenced by the low latitude Pacific Ocean SST anomalies. These SST anomalies, in turn, govern the interannual variability of the predictions in Figure 4.

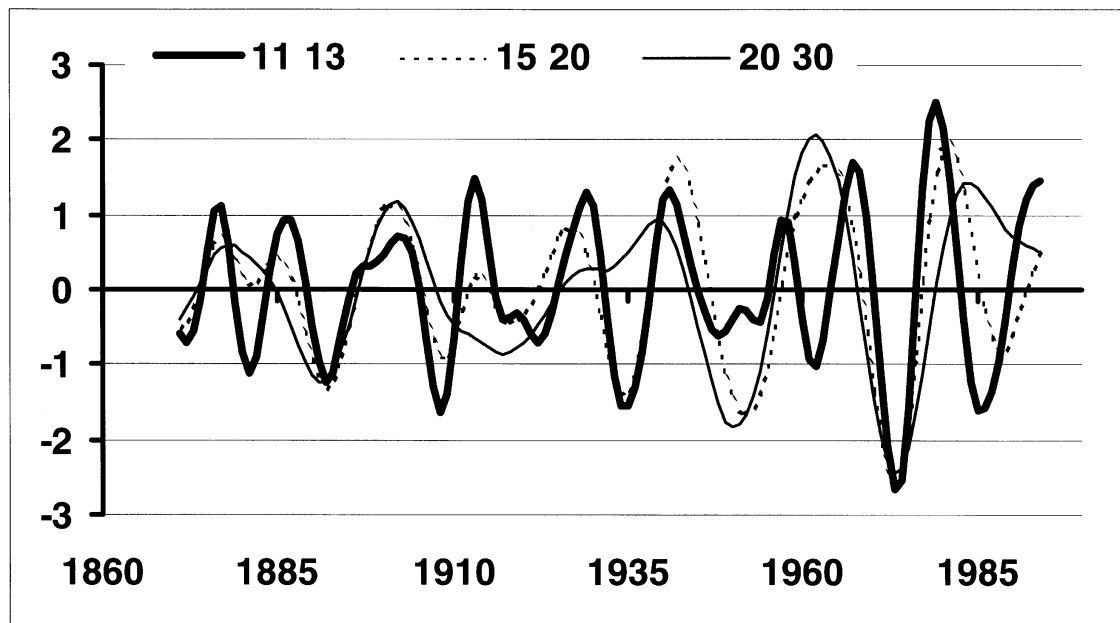


Figure 9 EOF1 time series of combined near global distributions of sea surface temperature and mean sea-level pressure, band-passed filtered for the periods 11-13 years, 15-20 years and 20-30 years.

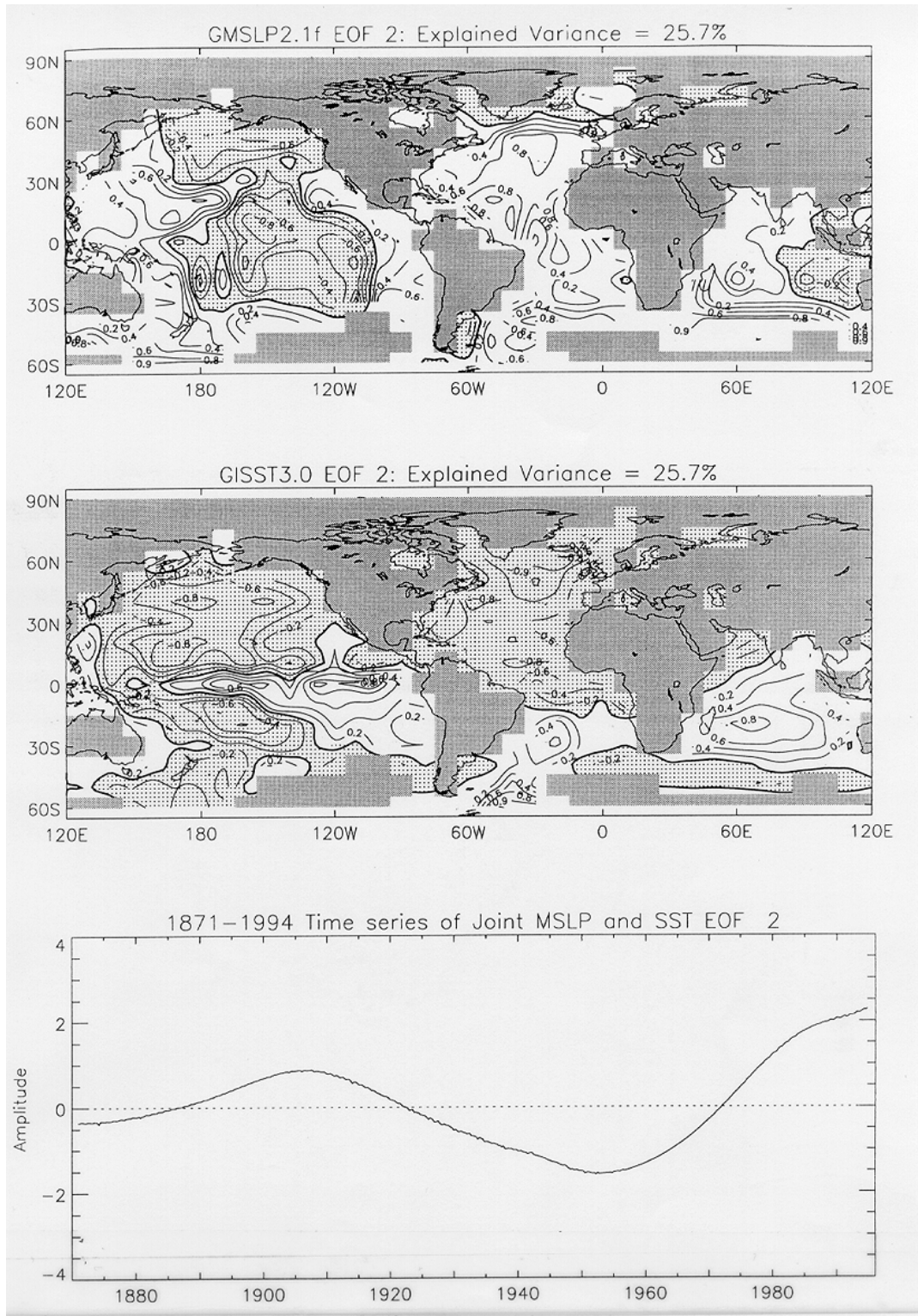


Figure 10 EOF2 of combined near global distributions of sea surface temperature and mean sea-level pressure, band-passed filtered for periods greater than 39 years. The upper panels show the spatial patterns and the lower panel shows the associated time series.

Table 1 Correlations between observed SWWA winter (JJA) rainfall and Perth MSLP, Darwin MSLP, Tahiti MSLP and the SOI, respectively

<i>Period: 1907-1994</i>			
	MAM	May	JJA
Perth	-0.16	-0.15	-0.83
Darwin	-0.08	-0.04	-0.31
Tahiti	0.14	0.15	0.31
SOI	0.14	0.00	0.34
<i>Period: 1950-1994</i>			
	MAM	May	JJA
Perth	-0.23	-0.17	-0.80
Darwin	-0.13	-0.15	-0.26
Tahiti	0.02	-0.02	0.33
SOI	0.09	0.00	0.31

Figure 11 shows the spatial distribution of the correlation between the observed MSLP and SWWA JJA rainfall for JJA, MAM and May alone conditions (left panels). The corresponding correlations for observed SST and SWWA JJA rainfall are illustrated in the right panels of Figure 11. In May, the centre of action between MSLP and SWWA rainfall in JJA is located well to the west of Australia, with maximum correlations of about -0.5 .

Unlike the situation for Perth in Table 1, over the southern Indian Ocean the MSLP for May has some implied predictability for SWWA JJA rainfall. In MAM, a more complicated spatial pattern with two nodes exists, one adjacent to Western Australia and the other in the central Indian Ocean. The related correlation coefficients are smaller and a more complex synoptic interaction over the ocean is implied. By JJA, the correlation pattern is largely centred over SWWA, as would be expected, with correlations exceeding -0.65 . While the MAM MSLP correlations in Figure 11 suggest a possible connection with north-west cloud bands, the May results indicate a higher latitude influence that could be associated with the Antarctic Circumpolar Wave.

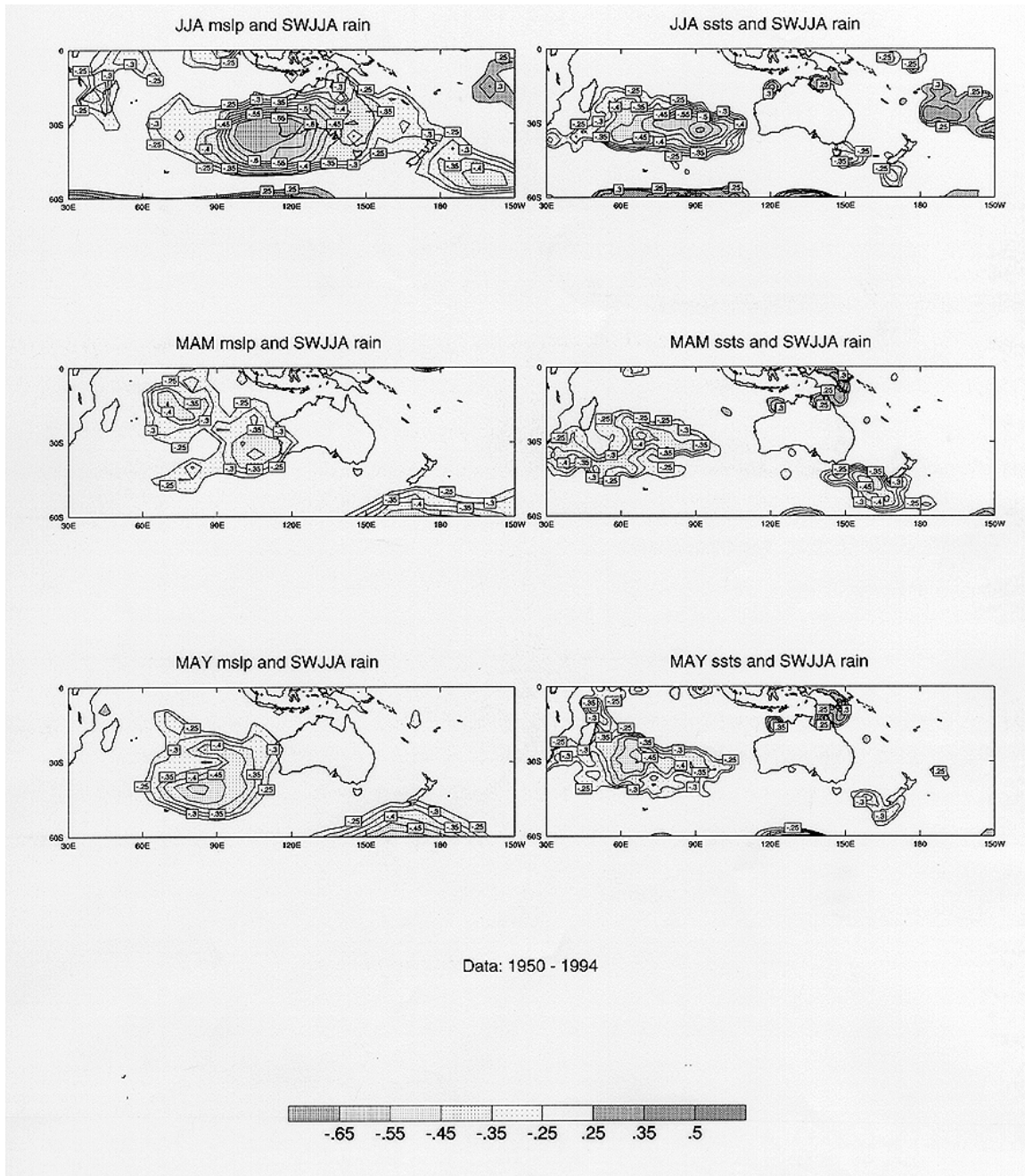


Figure 11 Spatial distributions of the correlations between MSLP and SST and SWWA JJA rainfall are shown in the left and right hand panels respectively. The top panels are for JJA conditions, the middle panels for MAM and the bottom panels for May alone conditions. The correlations are based on observations for the period 1950-1994.

In the case of SST, a more stable spatial pattern is apparent in Figure 11, with maximum correlations with SWWA JJA rainfall around -0.45 . The spatial pattern progresses somewhat eastwards between May and JJA conditions, but at all times is located to the west of the continent. Again the indication is for the major influence on SWWA rainfall to be located in the southern Indian Ocean, rather than connected directly with the SST dipole in the northern Indian Ocean, and thus the north-west cloud bands.

Finally, in Figure 11 the minor correlations with events in the low latitude Pacific Ocean is noteworthy, in agreement with the modest correlations with the SOI in Table 1.

An attempt was made to use the correlation results in Figure 11 to determine the predictability for JJA rainfall over the south-west. Using 10° by 10° boxes centred on the regions of maximum correlation for May shown in Figure 11, linear regressions were calculated between SWWA JJA rainfall and the preceding May MSLP and SST respectively, for the period 1950-1994. The resulting regressions were then used to generate the “fitted” curves in Figure 12, in which observed rainfall anomalies are compared with the rainfall anomalies obtained from the regressions. Very similar results were obtained with both approaches; the overall correlation being 0.5. Somewhat different temporal variations are apparent in the figure, but both approaches failed to capture the interannual extremes in observed rainfall.

In principle, the technique can be used to predict rainfall for later years, although high skill would not be expected. While the predictability of SWWA JJA rainfall, as presented in Figure 12, is not high, it would appear that if MSLP and SST variability over the southern Indian Ocean can be captured in a model, then some predictive skill should be obtainable. Quantification of such skill can be determined in future research.

(f) Synoptic study

An examination has been made of the ability of the T63 version of the CSIRO Mark 2 atmospheric global climate model to reproduce observed synoptic conditions over SWWA. Figure 13 shows a four-day sequence of observed rainfall over Western Australia and the adjacent oceanic region. This displays a large-scale system approaching from the west, producing intense rainfall over SWWA and propagating eastwards.

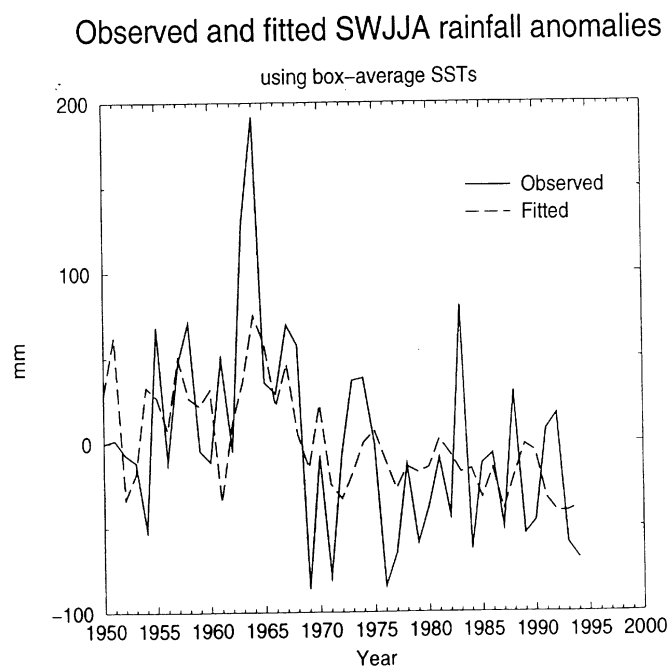
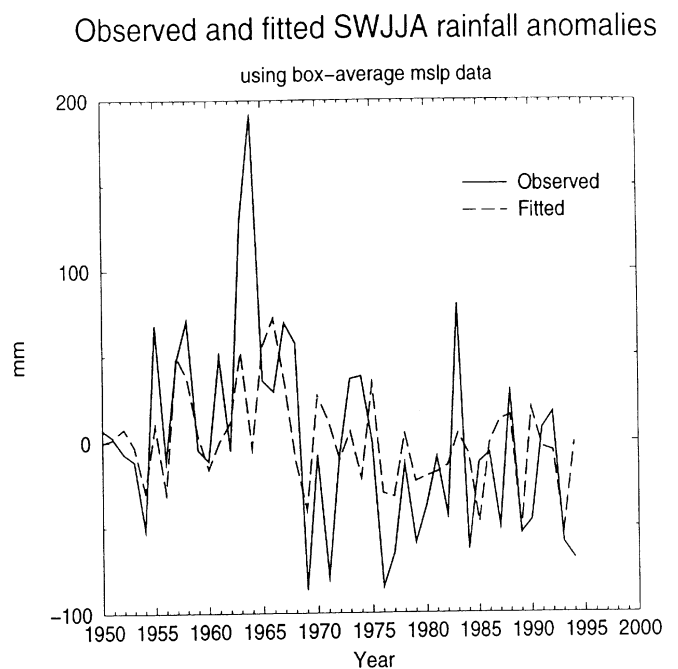


Figure 12 Observed and fitted SWWA JJA rainfall anomalies for the period 1950-1994. The fitted results were obtained by computing regressions between May MSLP and SST for 10° by 10° boxes centred over regions of maximum correlation for May in Figure 11, and then using the regressions to compute the results shown in the figure. The top panel is for MSLP and the bottom panel for SST.

In agreement with Figure 11, the *major* influence on the synoptic system shown in Figure 13 appears to derive from events over the southern Indian Ocean. However, the first panel of Figure 13 shows some linkage to the north-west cloud bands, implying that such bands may also influence SWWA rainfall, as is also suggested by Figure 7.

Similar systems were simulated in the model when it was forced with the GISST data set from 1871-1991. An example is given in Figure 14, where the 5-day sequence corresponding to 28 June - 2 July 1991, is shown for *each* of the four GISST simulations conducted. In all simulations a rainfall band progressed eastwards across the south-west, similar to the observations in Figure 13. Clearly, the model is capable of replicating this important feature of SWWA climatology. This is, of course, a prerequisite for any model-based multi-seasonal prediction scheme.

Due to chaos in the climatic system, noticeable differences exist between the four simulations for a given day. Consider, for example, the rainfall over SWWA on 30 June for the four simulations. In the first simulation, no dominant synoptic system prevails while in the second, the major system is located to the south and east of SWWA. In the third, a major frontal system is just reaching the coast of Western Australia, while in the fourth, a large frontal system extends diagonally across SWWA. Associated with these situations are substantially different synoptic pressure distributions, implying that independent synoptic events have been generated in the four simulations. All of the model runs were forced by the same global SST distributions, hence the differences between the sequences for a given day indicate that a given SST distribution does not produce a unique rainfall pattern. Although these results relate to the daily scale, they again emphasise the necessity of conducting multi-member ensembles for any planned multi-seasonal predictions. The temporal variability apparent in Figure 14 also highlights the problem of deciding at which time scale predictive skill become apparent. There is obviously none at the daily scale but there may be skill at the monthly or seasonal scale which match the time scales of the SST anomalies.

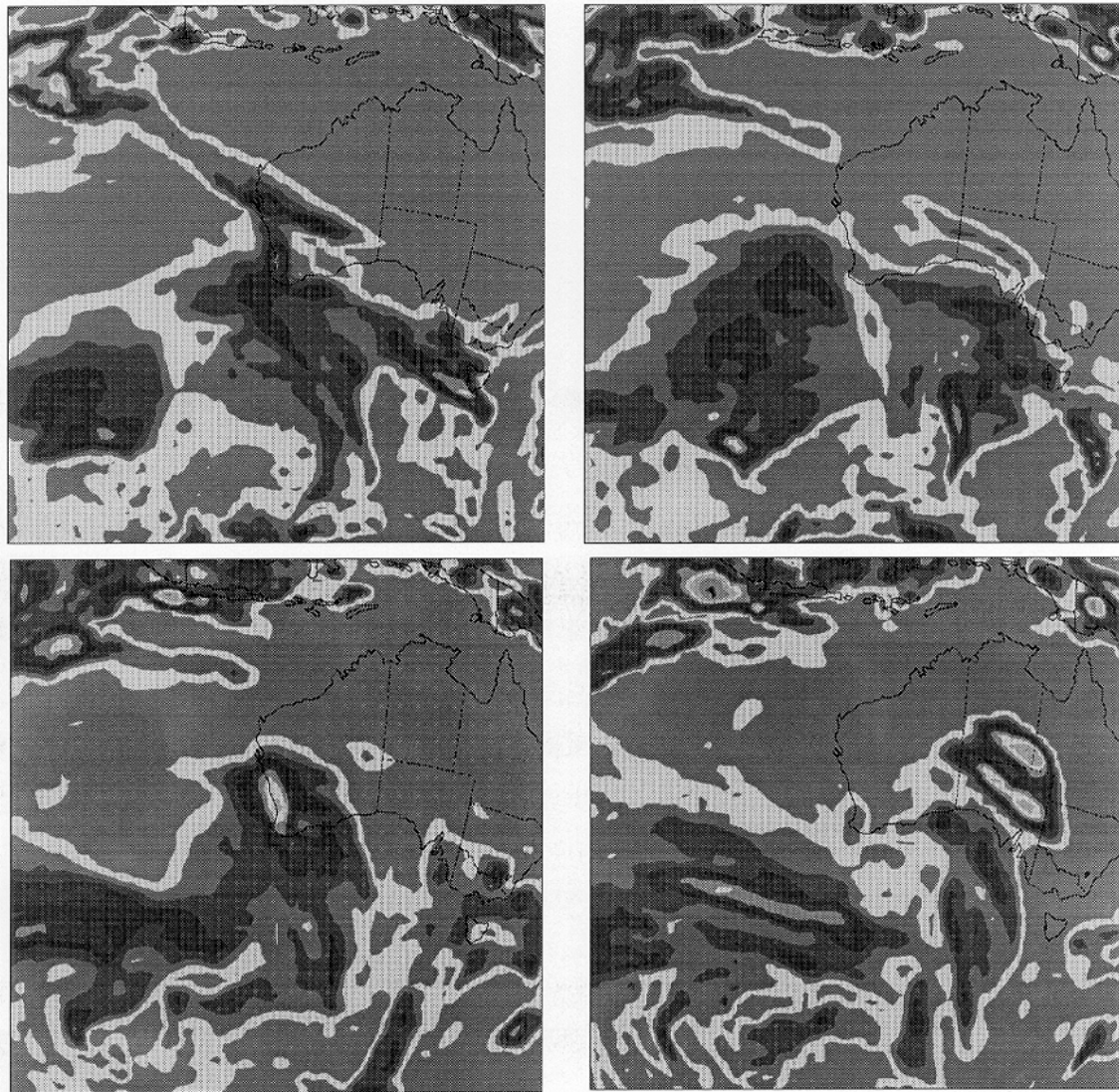


Figure 13 Sequence of 24-hour rainfall totals (mm) over the period 22-25 July 1996 according to NCEP/NCAR reanalysis data. 22 July (*upper left panel*), 23 July (*upper right panel*), 24 July (*lower left panel*) and 25 July (*lower right panel*). The black shading encloses values greater than 6 mm.

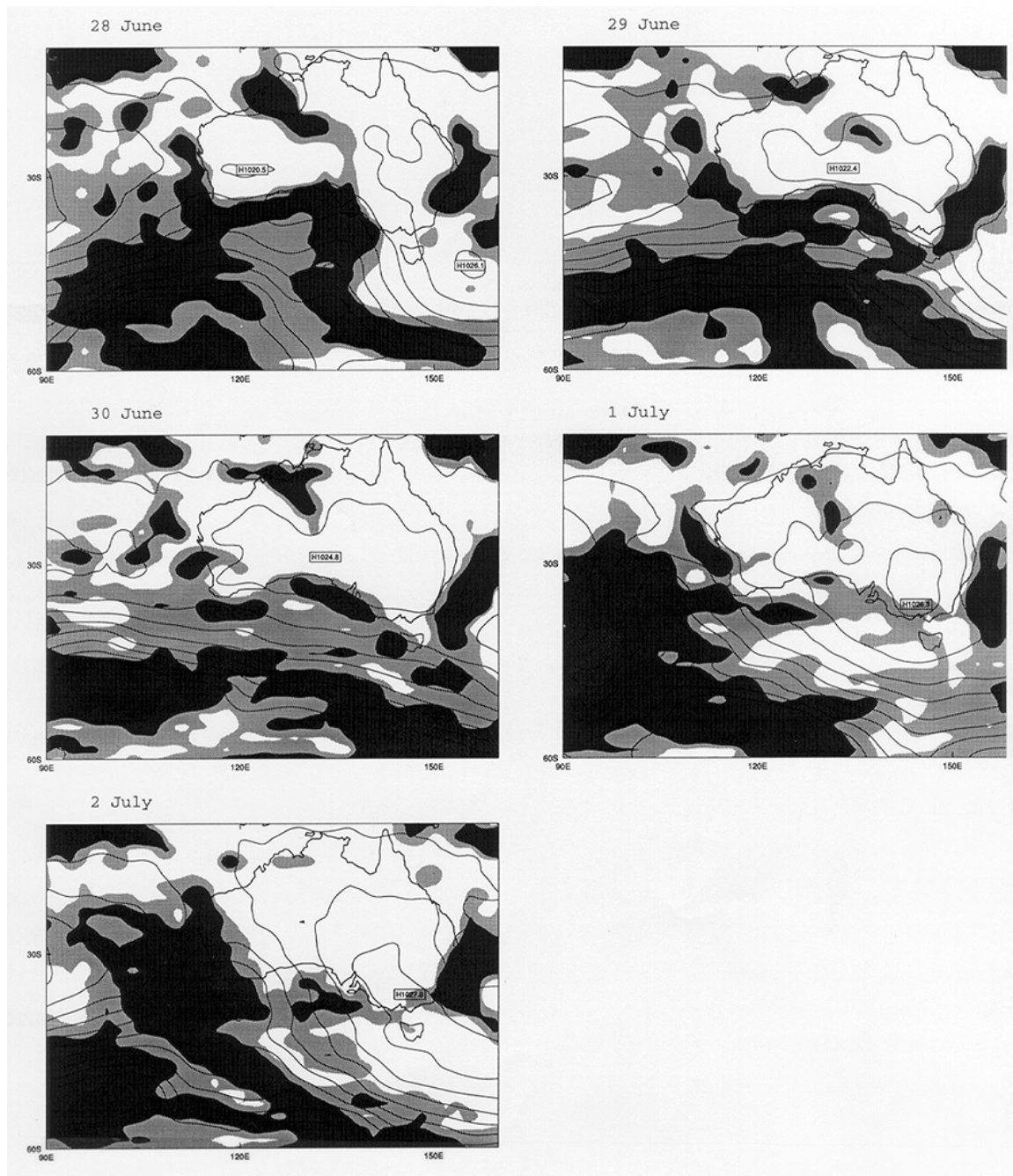


Figure 14 Five-day sequences of rainfall over Australia simulated with the CSIRO Mark 2 model forced with the observed GISST data set. Results are shown for four separate simulations, which differed only in the initial conditions used in 1871. Each individual page of the figure shows five consecutive days starting on 28 June 1991. The darker shading in the figure corresponds to heavier rainfall. In each panel the underlying surface pressure distribution is shown. *Simulation number 1.*

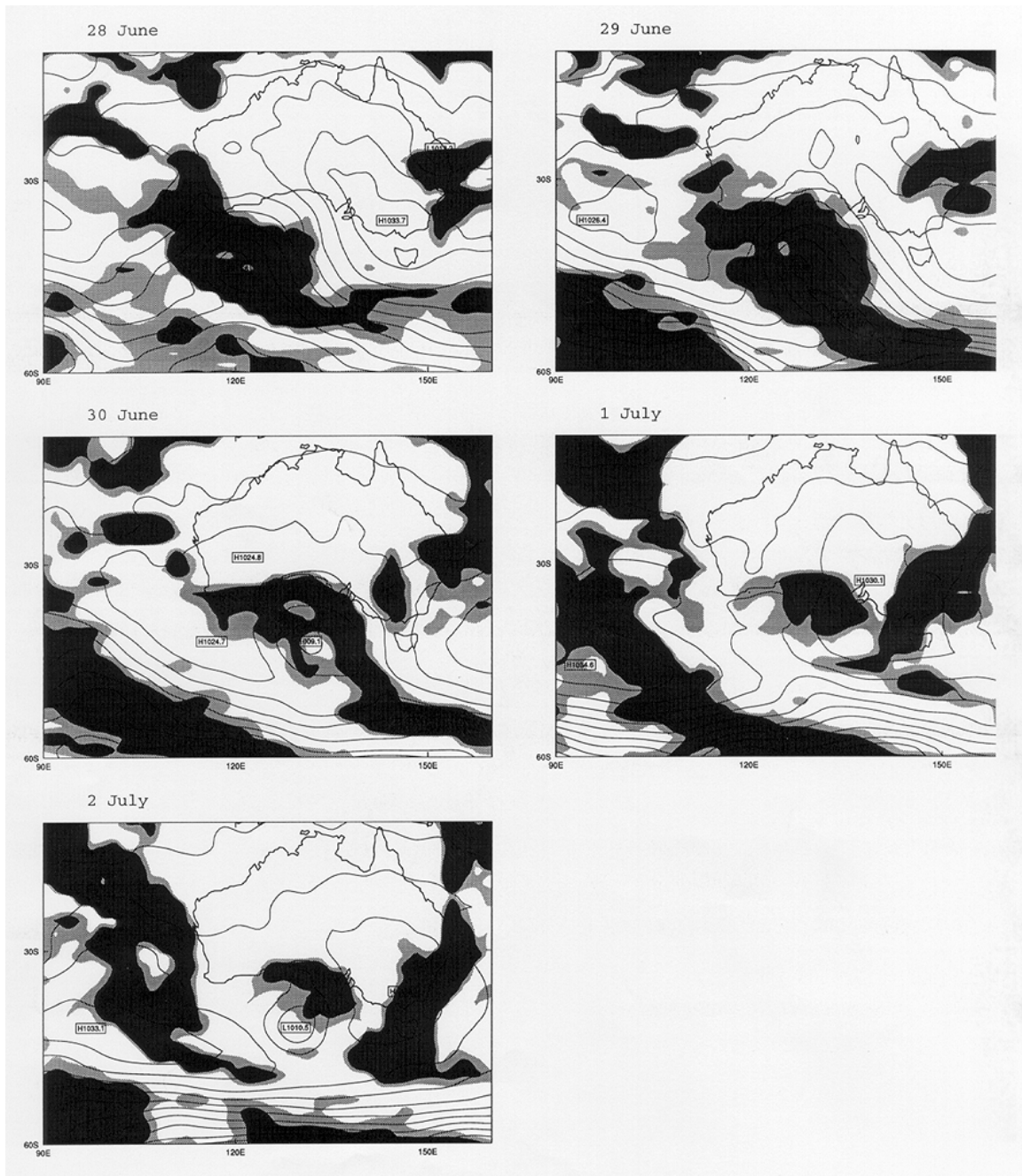


Figure 14 Continued. *Simulation number 2.*

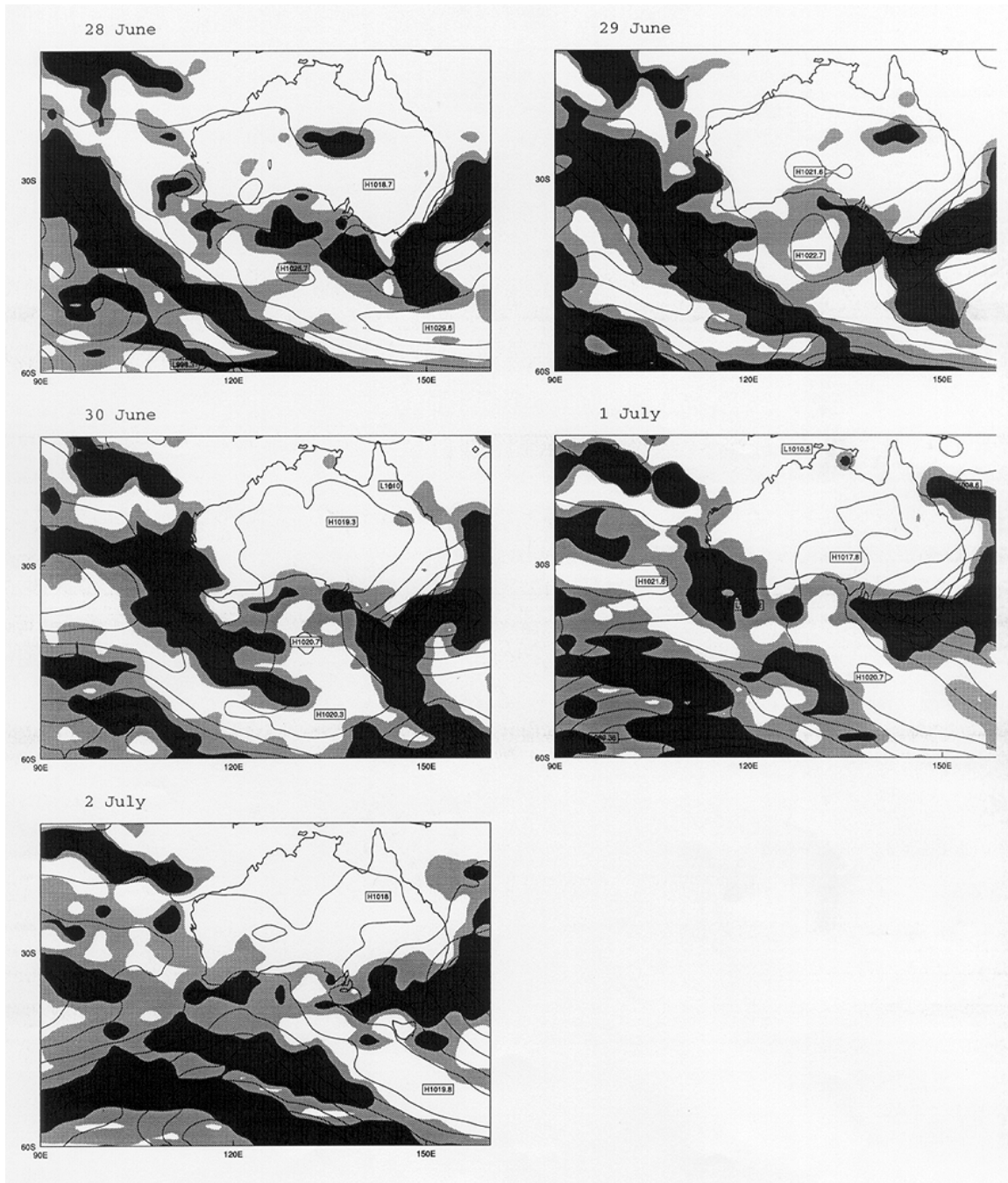


Figure 14 Continued. *Simulation number 3.*

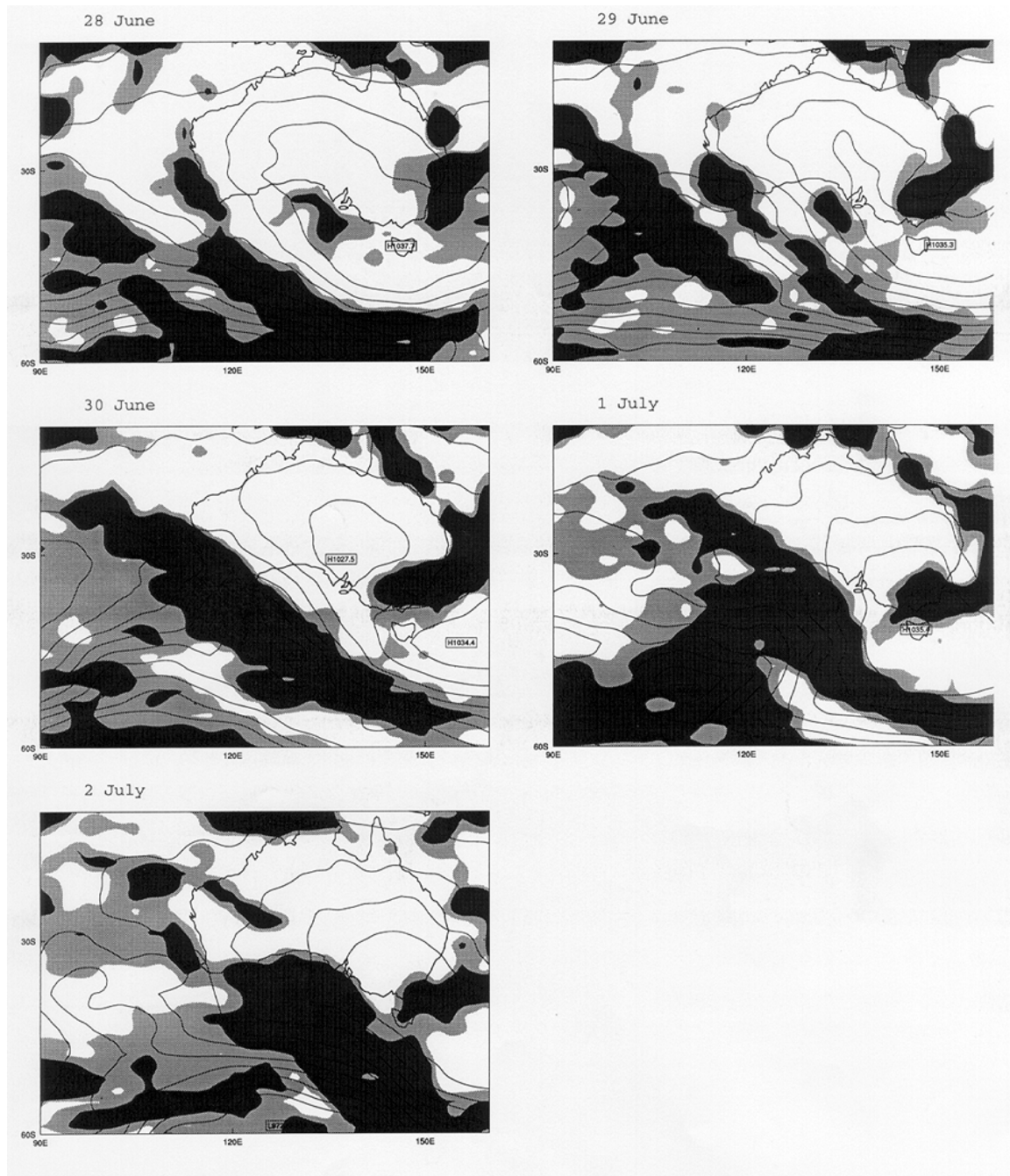


Figure 14 Continued. *Simulation number 4.*

(g) The CSIRO Mark 3 model

All of the results presented above have been based on the CSIRO Mark 2 global climate model in its various configurations. The Mark 3 version of the CSIRO model is now in its final evaluation stage, involving coupling of the atmospheric and oceanic components developed at CSIRO Atmospheric Research. Preliminary assessments suggest that this model will have a far superior performance to the Mark 2 model. It will be used in a wide range of climate-related assessments and can be applied to future Indian Ocean Climate Initiative Project research activities.

An indication of the atmospheric model's potential is illustrated in Figure 15, which shows a sequence of six continuous days of rainfall over the Australian region in January. The model was forced with a climatological SST distribution, so the results in the figure are not for any particular year. The horizontal resolution of the model is T63 ($1.875^\circ \times 1.875^\circ$) with 18 vertical levels.

Figure 15 shows in the first panel labelled Y19 M01 D02 (year, month, day) an intense rainfall event off the north-west coast of Western Australia, which is associated with a local low pressure system. In subsequent days (D03, D04 and D05), this system can be seen to move southwards and westwards and then eastwards as it becomes established over land (D05). Subsequently, the system degrades into an intense low pressure rainfall event ($\sim 50 \text{ mm day}^{-1}$) extending over the Kalgoorlie area, similar to tropical cyclone Vance earlier this year. In the final day shown (D07), the system progressed south-eastwards into the Bight as it decayed rapidly.

The sea-level pressure distributions associated with this event are shown in Figure 16 and, although similar to those of a tropical cyclone, lacked the extremely low pressures observed because of the coarse resolution of the model. A surface pressure of 987 hPa was reached in D04. A cross-section of this system displaying the wind intensity as a function of height revealed local wind values greater than 100 kph at 700 hPa height.

Mark 3 model performance shows the potential of the research tools that CSIRO will be able to apply to Indian Ocean Climate Initiative Project climatic problems in future.

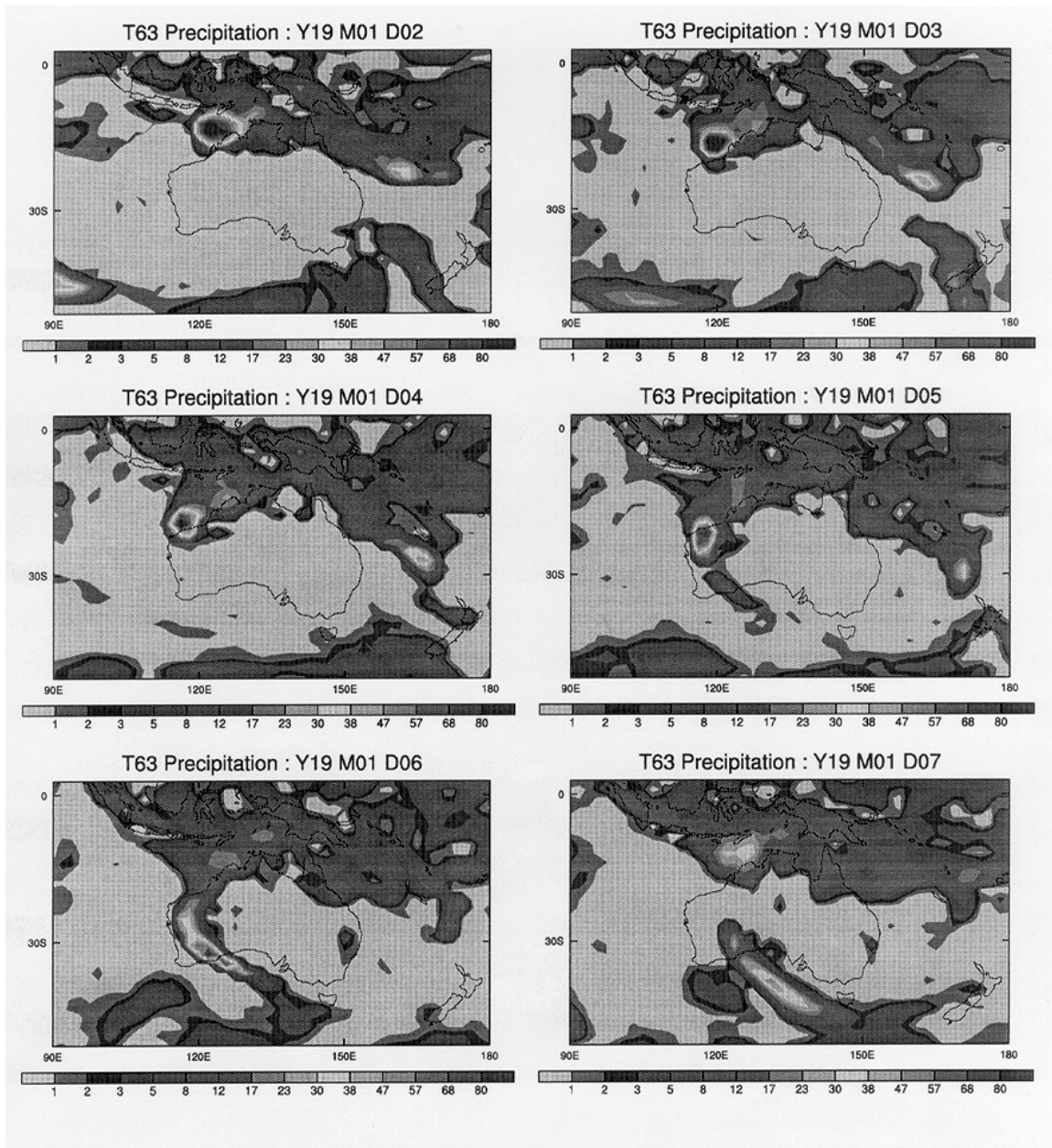


Figure 15 A six-day sequence of rainfall for the Australian region in January from the CSIRO Mark 3 model. The rainfall is associated with a ‘tropical cyclone’ type system. The rainfall is shown in mm/day.

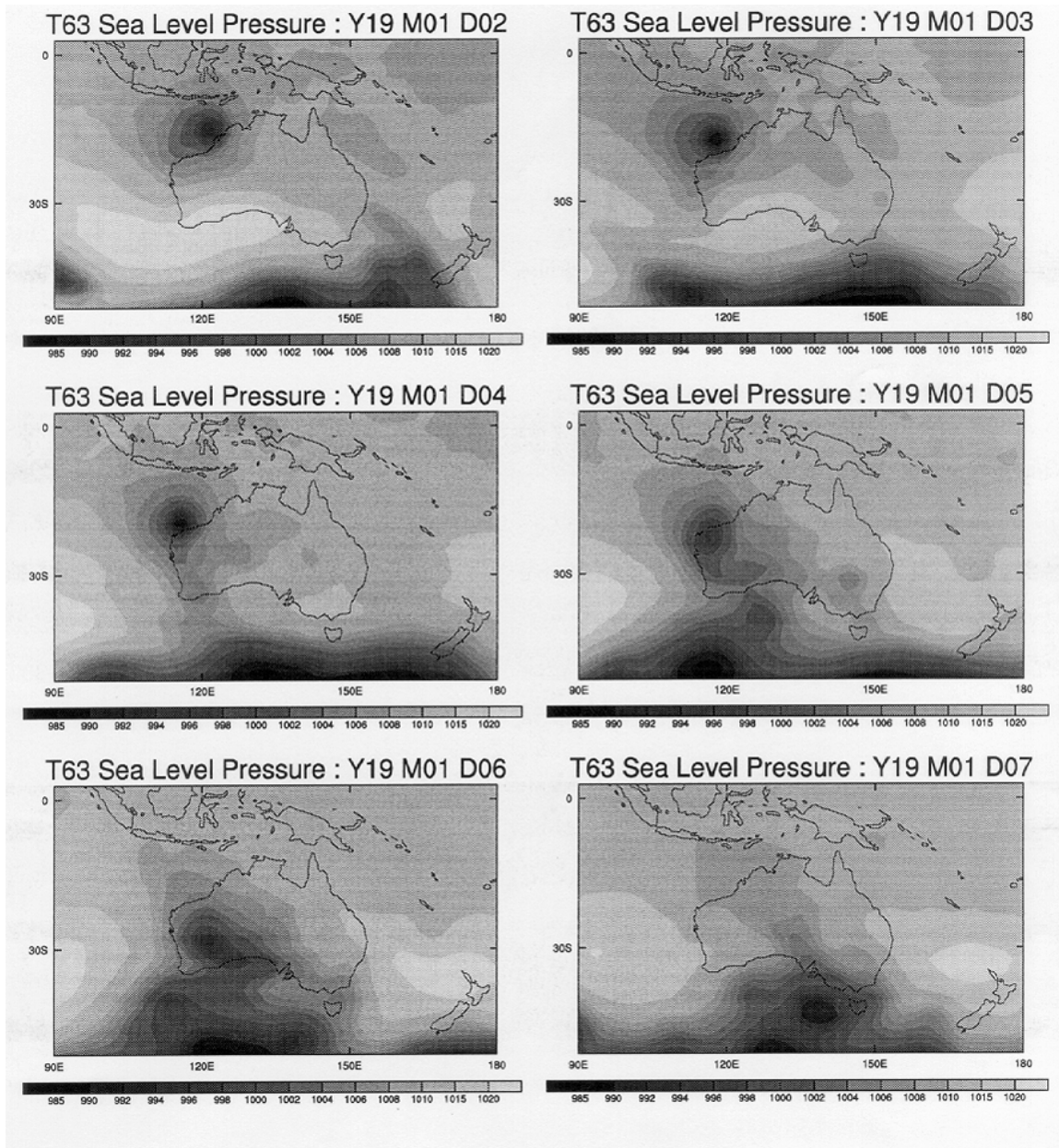


Figure 16 The sea-level pressure distributions corresponding to the rainfall sequence shown in Figure 15. The surface pressures are in mb.

Climatic trends

There are a number of examples of major climatic trends of varying duration and intensity. Two of the best known are the Medieval Warm Period and the Little Ice Age, which have generally been attributed to solar variations. A simple, and equally plausible, explanation is that these events are examples of natural climatic variability (Hunt, 1998). A climatic trend more relevant to Western Australia is the long-lasting drought in the Sahel. Again this event has been attributed to natural climatic variability (Hunt, 1999a), although rather complex climatic interactions appear to be involved. Thus, in considering the extended drying trend in SWWA, it is again appropriate to explore the role of natural climatic variability.

For the purposes of this exercise, natural climatic variability is defined to be the climatic anomalies that appear on an interannual and decadal (or even centennial) basis due to internal interactions within the climatic system. (Such internal interactions are caused by complex physical processes within a nonlinear climatic regime, with the non-linearity being the critical feature). By definition, phenomena such as solar fluctuations, volcanoes, and land use changes are excluded from consideration.

Natural climatic variability can then be studied by using a coupled atmospheric-oceanic global climatic model to produce an extended simulation of the present day climatic system. The Indian Ocean Climate Initiative Project has been able to capitalise on an existing 1000-year long climatic simulation conducted by CSIRO Atmospheric Research. This simulation was made for present day atmospheric carbon dioxide concentrations and no changes were permitted to the model in the course of the simulation. This report presents only annual mean results.

In order to obtain an appropriate perspective on the SWWA problem, a number of global-scale results will be presented. Results for trends, or runs of years, for a number of climatic variables will be considered. A 'hard' definition was used to define a trend. Thus, for a 10-year trend, this required that the same-sign climatic anomalies had to be recorded for all 10 successive years in the trend under consideration. The more common practice is to permit minor exceptions (i.e. 'soft' trends) where climatic anomalies of a different sign occur in the definition of a trend. Results for both types of trends will be presented.

Using the ‘hard’ definition of a trend, Figure 17 illustrates regions over the globe where positive or negative rainfall trends of either 10 or 12 years’ duration occur. Two immediate outcomes are apparent. Firstly, modelling suggests that 10-year duration rainfall trends owing to naturally occurring climatic variability are quite common on a global basis. Trends of longer duration are much less frequent. Secondly, there is an asymmetry between the occurrence of positive and negative trends, with the latter predominating. Figure 17 indicates that 10-year drying trends occur over most of Australia in the 1000-year period considered.

Since rainfall variability, at least at ENSO frequency, is related to SST perturbations in the Pacific Ocean it is also useful to investigate trends in temperature. Figure 18 shows the proxy screen temperature (i.e. temperatures at a height of 10 meters above the surface) results for 15-year positive and negative trends. The spatial pattern is quite distinct from that of rainfall in Figure 17, and of longer duration. The major trends are located in the Pacific and Southern Oceans — the lack of an Indian Ocean signal is noteworthy.

The possibility that the above trends could be attributed to random effects, implying no associated physical mechanisms, was investigated by generating global distributions of random numbers for a 1000-year period. The same analysis procedure as used for the climatic variables was then applied to the random numbers. As expected, no asymmetries between positive and negative trends or preferential geographical regions were identified. A much more uniform spatial pattern was obtained with a somewhat reduced frequency of occurrence for 10-year trends. For 12-year trend periods, the frequency of occurrence was much less than shown in the lower panels of Figure 17, with mainly single grid boxes involved. These results suggest that 10- or 12-year rainfall trends can be expected at least once in 1000 years simply due to chance. However, the observed trends are of much longer duration and so this explanation is less likely.

Trends in other climatic variables were also examined. Because of the possible relationship between SST anomalies and zonal surface wind stress, the latter variable was investigated in some detail. The duration of trends was intermediate between those of rainfall and screen temperatures, with substantial regions having 12-year trends. Most such regions were located over the oceans, especially at low latitudes.

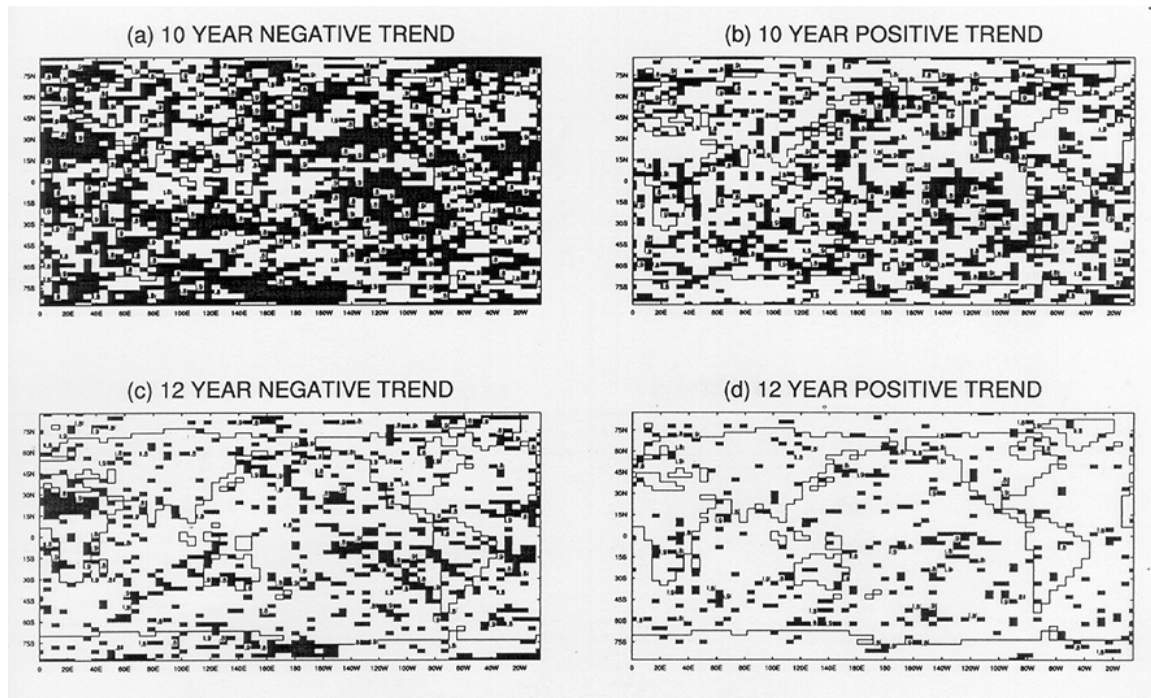


Figure 17 Locations where rainfall trends of a given duration were found at least once in the 1000-year simulation are identified by black rectangles. The upper panels show negative and positive trends of 10-years duration in the left and right hand panels respectively. The lower panels repeat this information for trends of 12-years duration.

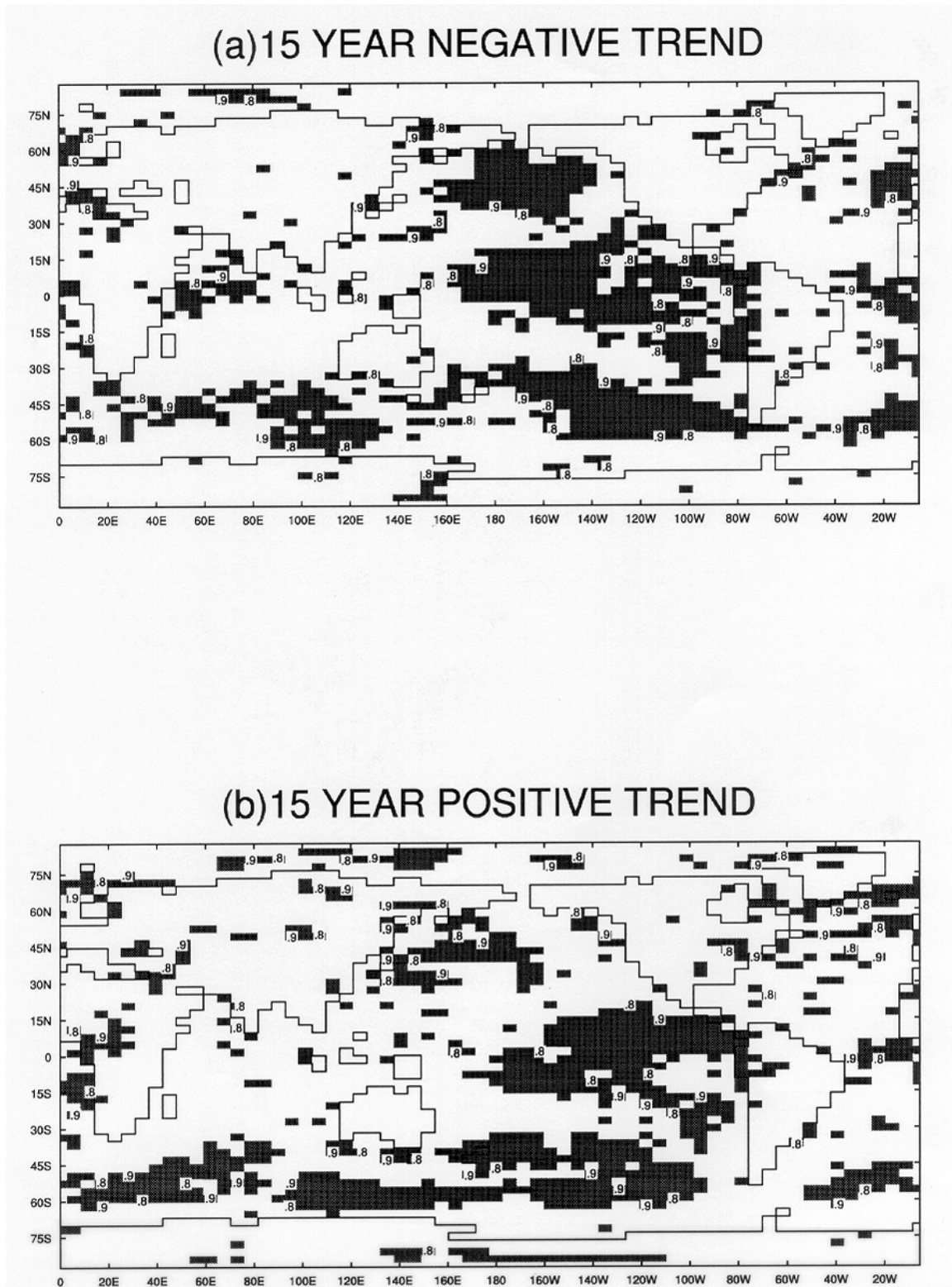


Figure 18 Locations where screen temperature trends of 15 years duration were found at least once in the 1000-year simulation are identified by black rectangles. The upper panel shows results for negative 15-year trends, the lower panel for positive 15-year trends.

While Figure 17 identifies regions where rainfall trends are to be expected, the figure does not reveal how frequently such trends occurred in the 1000-year simulation. Figure 19 shows the return period of positive or negative 10-year rainfall trends. Again an asymmetry is apparent, as well as preferred regions of occurrence.

Figure 19(b) indicates that very few model grid boxes experienced more than one positive 10-year rainfall trend in the 1000-year simulated period, the principal exception being in the central Pacific Ocean where up to three separate 10-year trends occurred in this period. Multiple 10-year trends for given grid boxes were much more frequent for negative rainfall trends (Figure 19(a)), with such events predominating in the Saharan region. The corresponding analysis, using random numbers, identified a number of grid boxes where up to two 10-year trends occurred, but with no spatial coherency. Approximately five grid boxes were found to have three 10-year trend periods. Thus in the case of rainfall, with the exception of the Sahara, rainfall deficits lasting more than 10 years are an unusual feature and have a return period of 1000 years. This conclusion is based on the ‘hard’ definition of a trend.

In the case of screen temperature, the percentage occurrence plot corresponding to Figure 19 reflected the spatial distribution of Figure 18. For 15-year duration trends (Figure 20), there are regions to the south of Australia where from three to five occurrences of such trends were identified within the 1000-year simulation. This implies return periods of from 200 to 333 years. As will be shown below, anomalies in screen temperatures are closely related to corresponding anomalies in SST and oceanic temperatures, hence the length of such trends. Such persistent SST anomalies may have an influence on circulation patterns over Australia and thus rainfall anomalies.

An important consideration in identifying relationships between climatic variables is the simultaneity of responses for a given region. This was investigated in the 1000-year simulation by selecting a temporal window — years 600-625 — and searching for grid boxes in the model where 10-year negative trends in anomalies for screen temperature, rainfall and surface wind stress occurred (see Figure 21). As might be expected from Figure 18, the dominant response was for screen temperature (Figure 21(a)), with a large region in the low latitude Pacific Ocean being identified. The rainfall and wind stress responses were progressively smaller, but in both cases registered effects in the low latitude Pacific Ocean.

While this behaviour doesn't establish cause-and-effect — appropriately designed experiments would be needed for that — the fact that some spatial coherence existed between the various climatic variables in Figure 21 does suggest a physical relationship.

The results in Figure 21 are for a particular temporal window— years 600-625 — and illustrate a single period. The variability of the trend characteristics with time is demonstrated in Figure 22, where three 25-year temporal windows were selected. For each of these windows, a search was made for 10-year trends in negative screen temperature anomalies. Quite clearly there is secular variability in the trend characteristics, both as regards the number of grid boxes identified with the trends and especially as regards their locations. This is an important fact which needs to be borne in mind when considering observed climatic trends for any given region.

Another important factor that needs to be quantified is the magnitude of the change in a climatic variable in a given trend period. Figure 23 illustrates the percentage rain loss or gain *per year* associated with negative and positive 10-year rainfall trends respectively. Again an asymmetry exists between positive and negative trends with far higher impacts associated with the latter. Annual anomalies corresponding to 20-30% of the long-term average appear to be quite common during the negative trends. While the biggest losses occur over the Sahara, it is Australia as a continent that registers the biggest areal affect! This result is attributed to the extensive arid or semi-arid regions in Australia compared with other continents. The biggest losses over land in Figure 23(a) are associated with desert regions, implying a mechanistic process, rather than random effects.

A useful indicator of the long-term consequence of drying and wetting trends is to compute cumulative anomalies of rainfall. Such anomalies are shown in Figure 24 for three locations in Australia. An interesting feature of this figure is the quite distinct responses for these regions over the 1000-year periods, suggesting that different climatic forcing mechanisms operated in the three regions. The characteristic feature of all three plots in Figure 24 is the high frequency variability superimposed upon long-term (multi-century in some cases) responses. From a hydrological perspective, this indicates that the integrated effect of intermittent, but persistent, rainfall trends is to create deficits or surpluses with surprisingly long-term characteristics. In regions where water supplies are being obtained from aquifers, available water could be affected by events that occurred decades or centuries earlier.

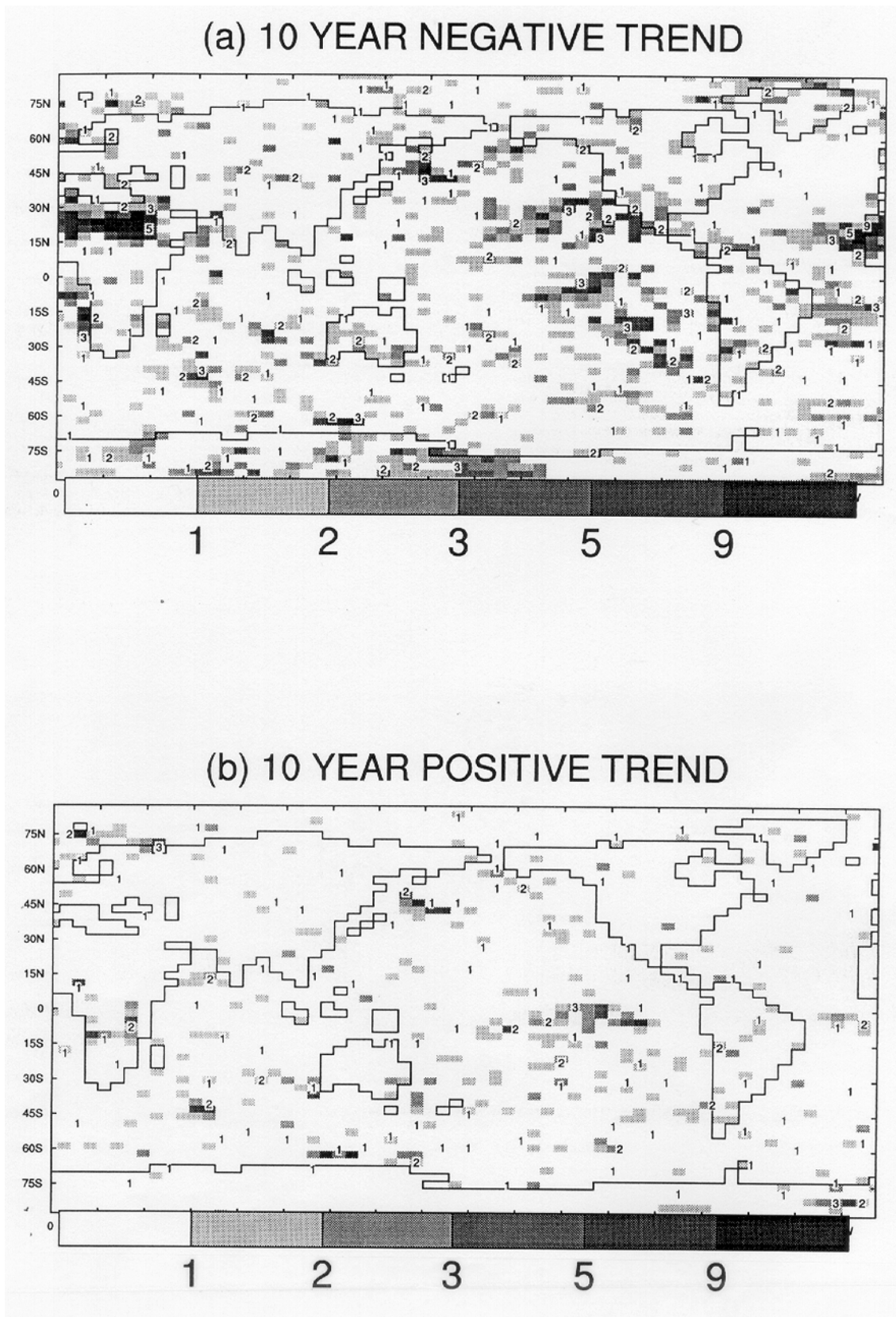


Figure 19 Locations where multiple rainfall trends of 10-years duration were found in the 1000-year simulation are identified by rectangles. Results for negative 10-year trends are shown in the upper panel, for positive 10-year trends in the lower panel. A rectangle identified with, say, 3, indicates that there were three 10-year periods found in the 1000-year simulation, implying a return period of 333 years.

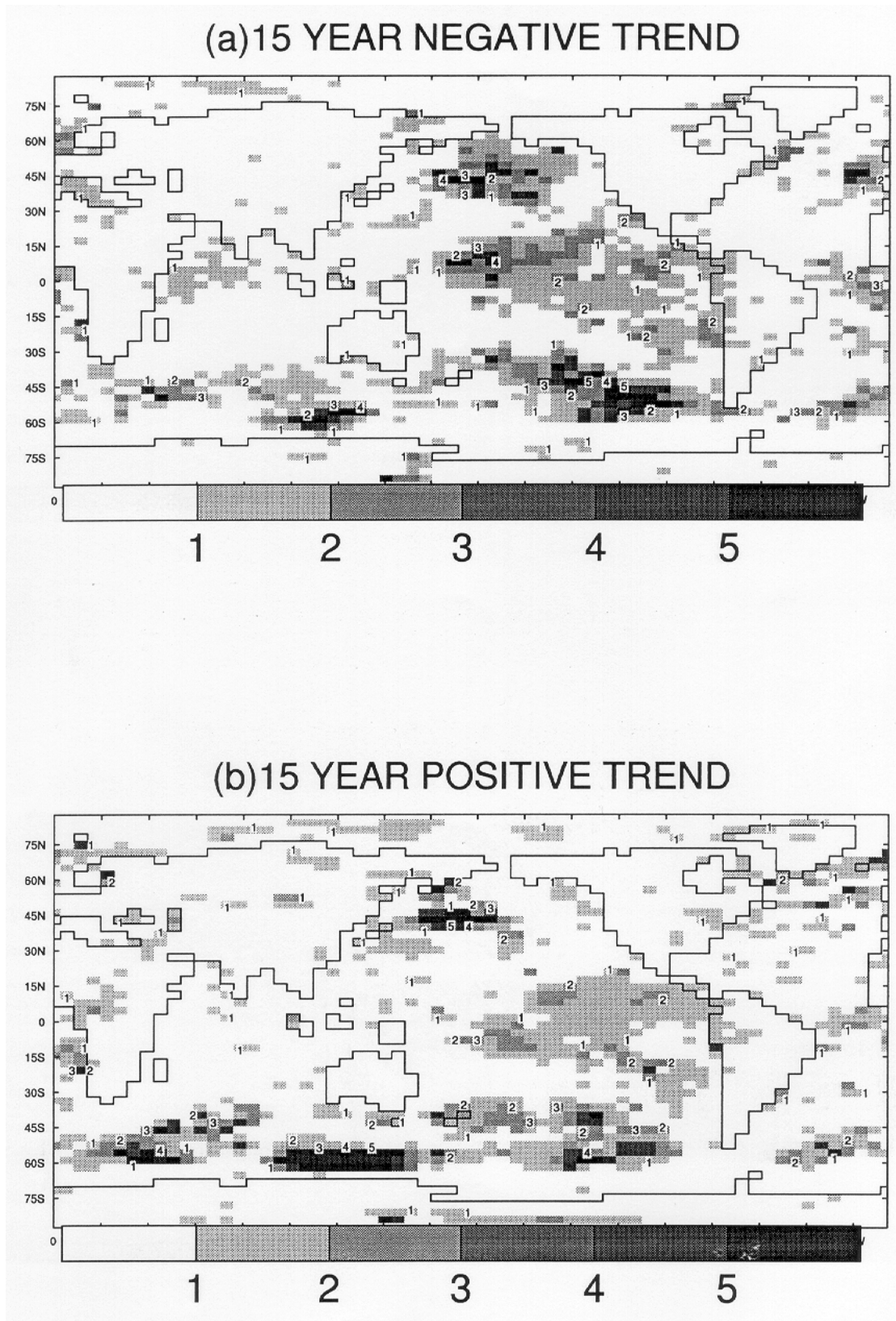


Figure 20 As for Figure 19, only for 15 year screen temperature trends.

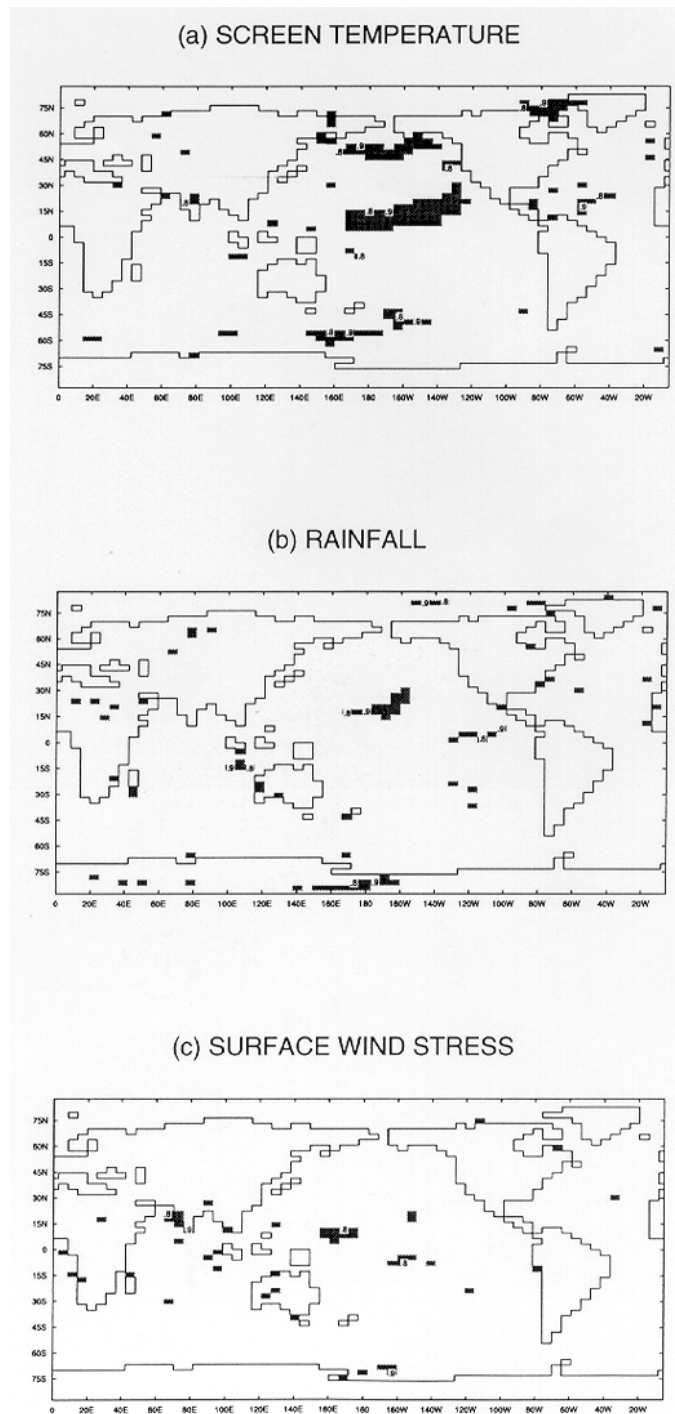


Figure 21 Locations where screen temperature, rainfall and surface wind stress with 10-year negative trends occurred in the timeframe 60-625 years of the 1000-year simulation are shown by black rectangles.

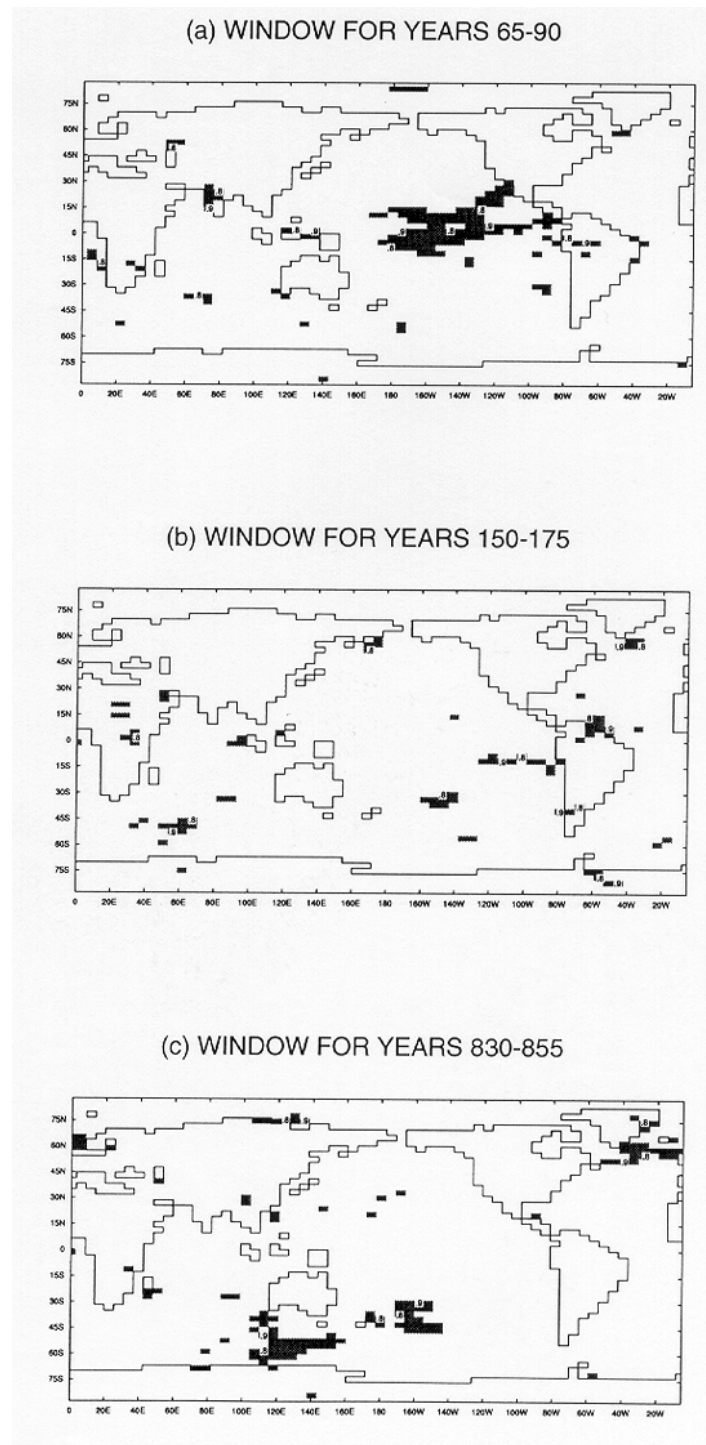
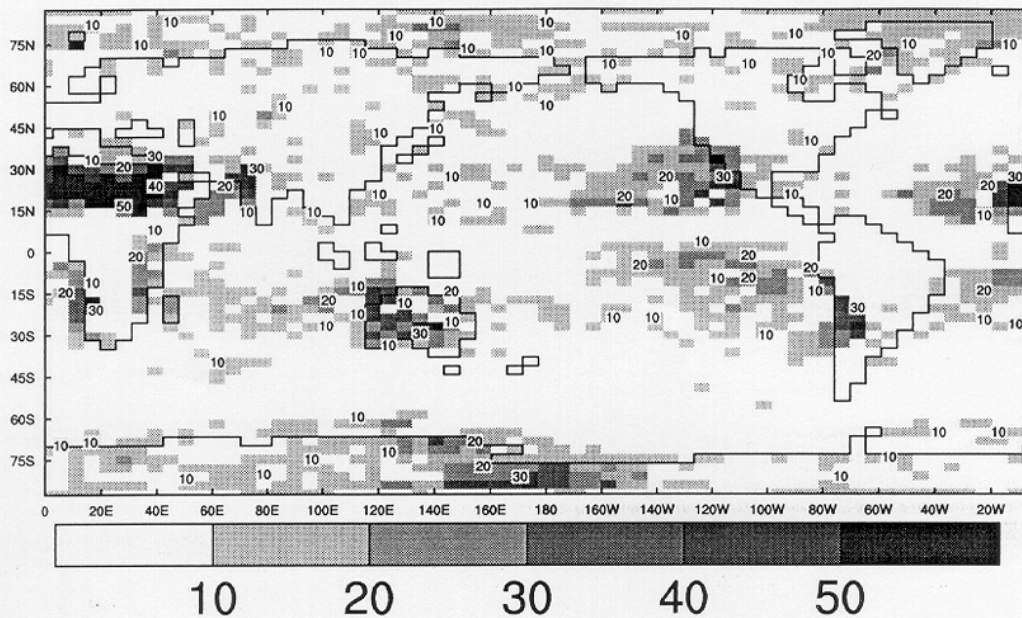


Figure 22 Locations where negative 10-year trends of screen temperature occurred in three separate 25 year periods are shown by black triangles. The individual periods are identified on each panel.

(a) Percentage rain loss per year for 10 year negative trend



(b) Percentage rain gain per year for 10 year positive trend

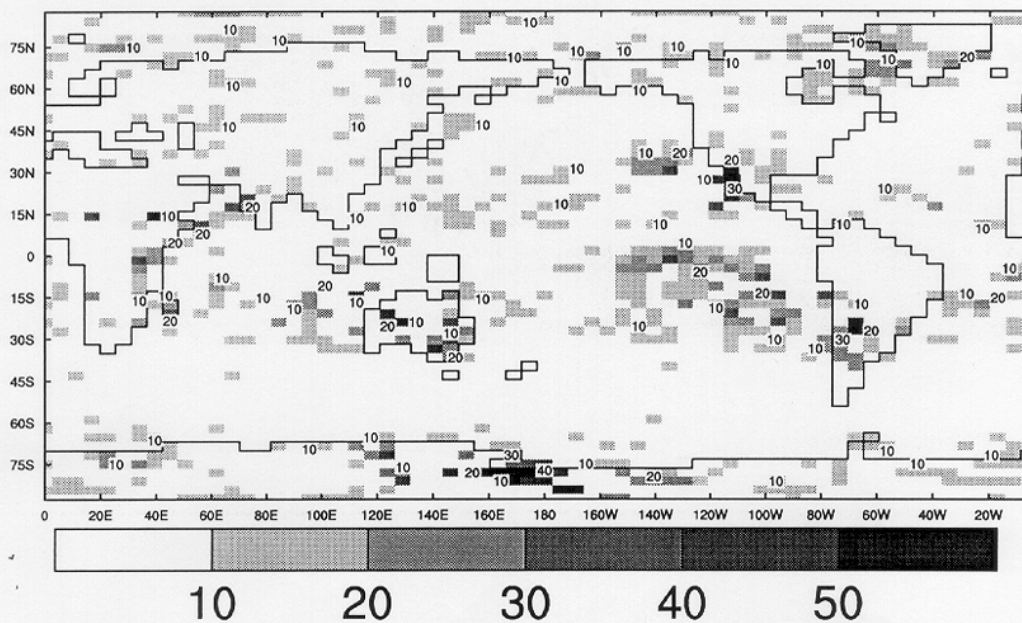


Figure 23 The percentage rain loss per year for negative and positive 10-year rainfall trends are shown in the upper and lower panels respectively.

Cumulative anomalies – Rainfall

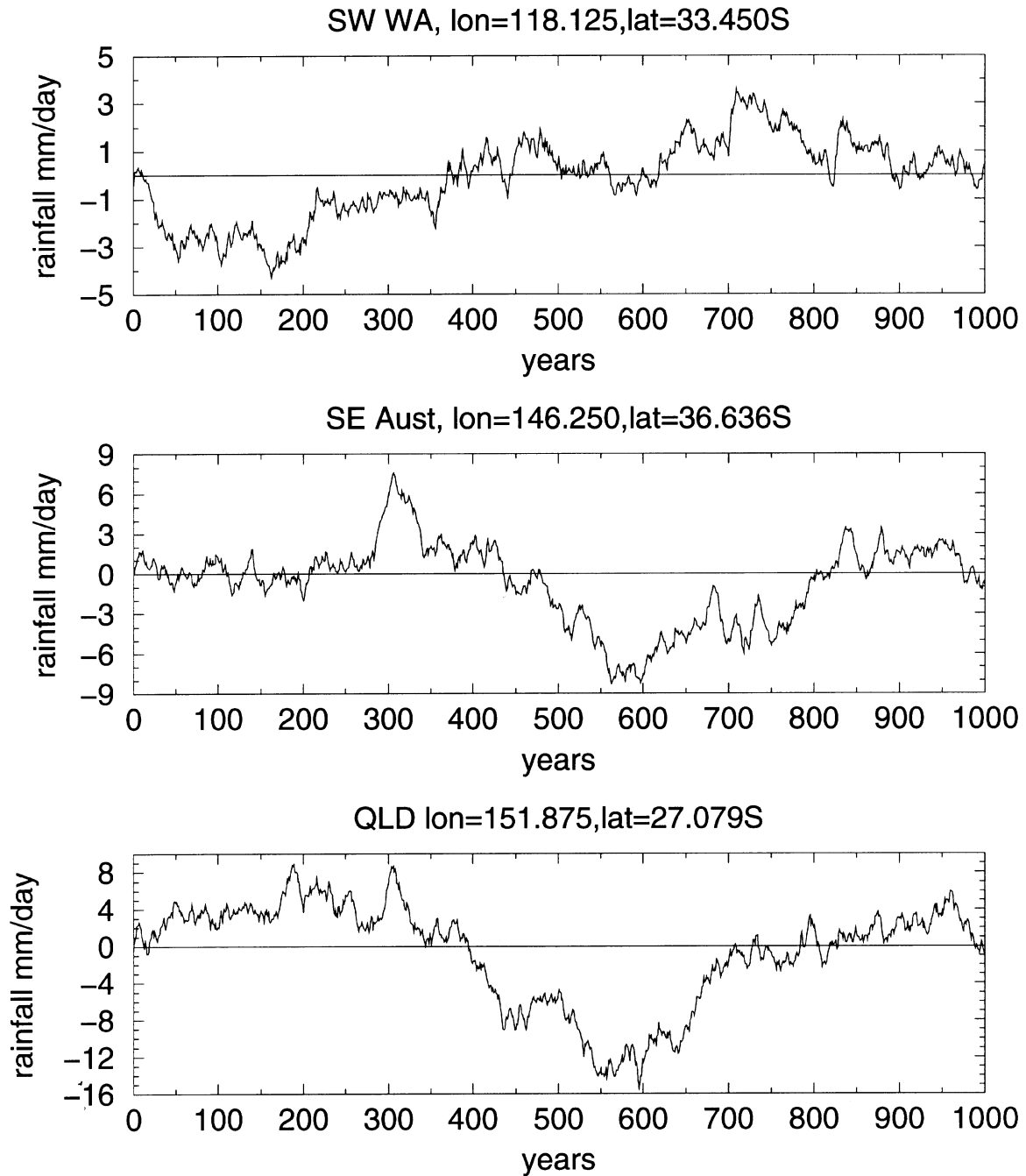


Figure 24 Cumulative rainfall anomalies for three model grid boxes, identified by longitude and latitude in the individual panels, from the 1000-year simulation.

A clearer picture of temporal variability of climatic anomalies can be obtained by plotting histograms of such anomalies, as given in Figure 25 for annual rainfall in a single grid box in central Pacific Ocean. This region is dominated by high frequency ENSO events, even though in the model such events are rather weak. Thus, the model simulation may inadequately represent reality. Nevertheless, this is a critical region for excitation of global climatic anomalies, so it is useful to investigate its behaviour prior to considering results specifically for SWWA. The time series in Figure 25 exhibit a range of responses from large amplitude decadal variability (years 250-500) to small amplitude interannual variability (years 870-970). There are four events that meet the 'hard' definition of a 10-year anomaly, centred approximately on years 60, 320, 670 and 870. Importantly, there are other, more extensive events, that can be considered to represent persistent trends if a looser definition of a trend is adopted. For example, there is a 19-year positive trend centred on year 340, a 15 year negative trend centred on a year 870, and a 34-year negative trend centred on year 720.

Results for SWWA are shown for a single grid box in Figure 26. The time series in this region have more interannual variability, but rather larger amplitudes compared with Figure 25. While there is only one 10-year 'hard' drying trend there is an almost 50-year drying trend at the start of the simulation. This is reflected in the cumulative anomaly time series in Figure 24. The long time frame required to recover from this initial drying trend is apparent in that figure. Other less consistent and persistent drying trends can be identified in Figure 26, and these are also reflected in Figure 24 where the positive runs of accumulative rainfall anomalies undergo multi-decadal reductions.

Time series plots were made for a number of other regions. Overall characteristics were similar except for a tendency to exhibit somewhat more decadal variability compared to the prevailing interannual variability in Figure 26. The amplitudes also varied, with anomalies of up to 1.5 mm day^{-1} occurring, for example, over East Africa.

Thus, compared to other regions there appears to be nothing extraordinary about the long-term rainfall variability over south-west Western Australia as far as simulations of natural variability are concerned.

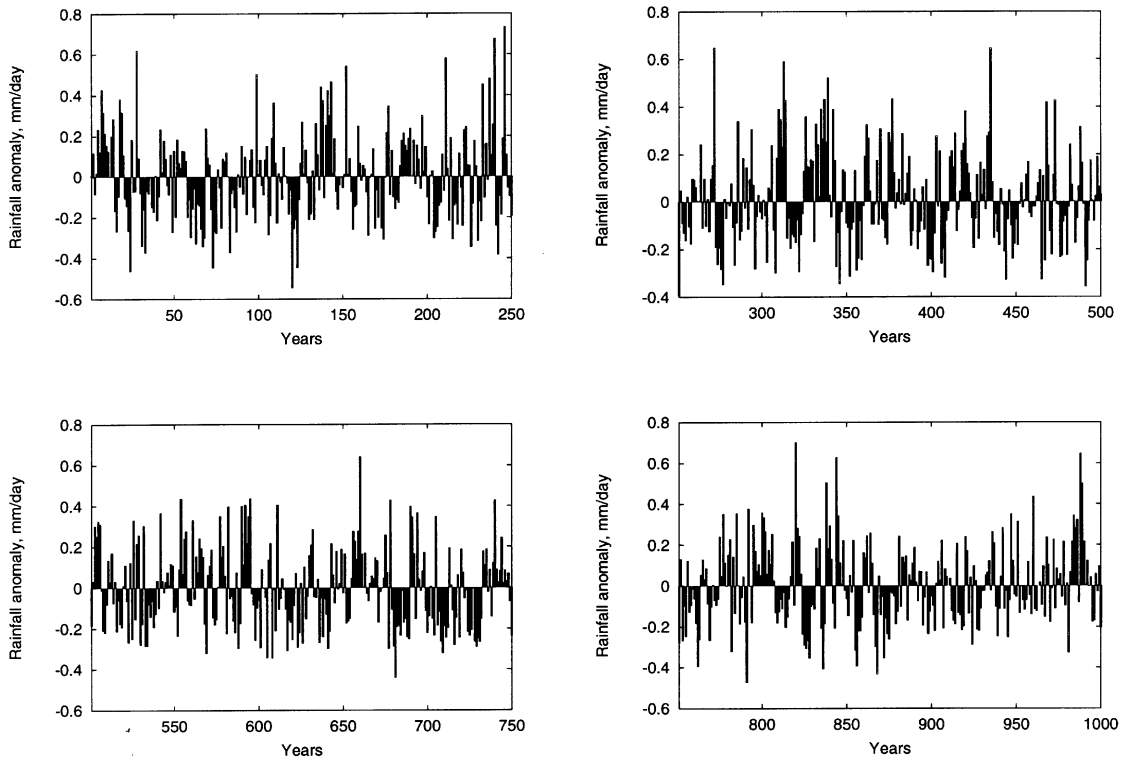


Figure 25 Histograms of annual rainfall anomalies from the 1000-year simulation for a model grid box in the central Pacific Ocean.

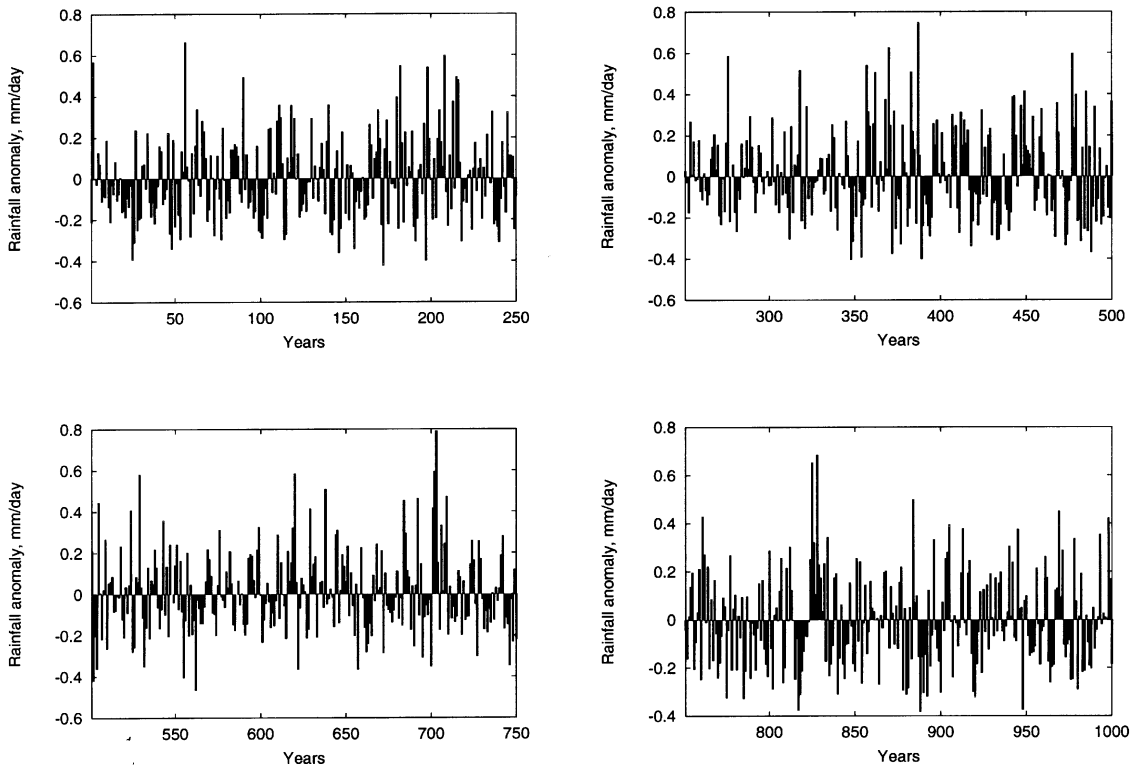


Figure 26 Histograms of annual rainfall anomalies from the 1000-year simulation for a model grid box in SWWA.

For convenience, single grid boxes have been used in the above temporal analysis. The representativeness of such boxes was assessed for a low latitude Pacific region and SWWA by correlating the rainfall anomaly time series for the selected box and 9-box and 25-box areas centred on such boxes for all 1000 years of the simulation. For the Pacific Ocean, the correlations were 0.96 for boxes 1 and 9 (1:9), 0.89 for 1:25 and 0.97 for 9:25. Over SWWA, the corresponding correlations were 0.78, 0.66 and 0.93. All these correlations are very highly significant because of the use of 1000 years of data. Over shorter time series, these correlations could be expected to vary more, but these results indicate that the mechanisms producing the anomalous rainfall variations generally operated over synoptic scales.

Given the important role of SST anomalies in generating climatic anomalies mentioned above, time series of anomalies of screen temperatures and oceanic temperatures were also examined. Results for SWWA are shown in Figure 27. These results were fairly typical of other land regions examined. As would be expected from Figure 18, somewhat longer term trends are more apparent than they were for rainfall. Anomalies greater than 0.5°C occur frequently and the related opposite trends can be broadly identified with the corresponding rainfall anomalies for SWWA in Figure 26.

Anomalies of SST show more persistent trends and, in some cases, much larger amplitudes. Figure 28 and Figure 29 show two examples. The SST anomalies in Figure 28 for the south Pacific Ocean reveal several multi-decadal trends, commencing with a 50-year cold trend. A warming trend, almost as long, is centred on year 330. Such persistent anomalies can be expected to generate related climatic anomalies in the atmosphere, with possible teleconnections to more distant regions. The results for the Southern Ocean in Figure 29 are closer to Australia longitudinally than those in Figure 28. They are exceptional, with large amplitude, short duration negative anomalies followed by sharp transitions to smaller amplitude, decadal or longer positive anomalies. The initial anomalies in Figure 29 were associated with a very large-scale SST anomaly at high latitude extending around most of the hemisphere. Whether, and how, such SST anomalies feed back into atmospheric climatic perturbations and possibly influence SWWA is unknown, as the high latitudes are ‘noisy’ regions in a climatic sense.

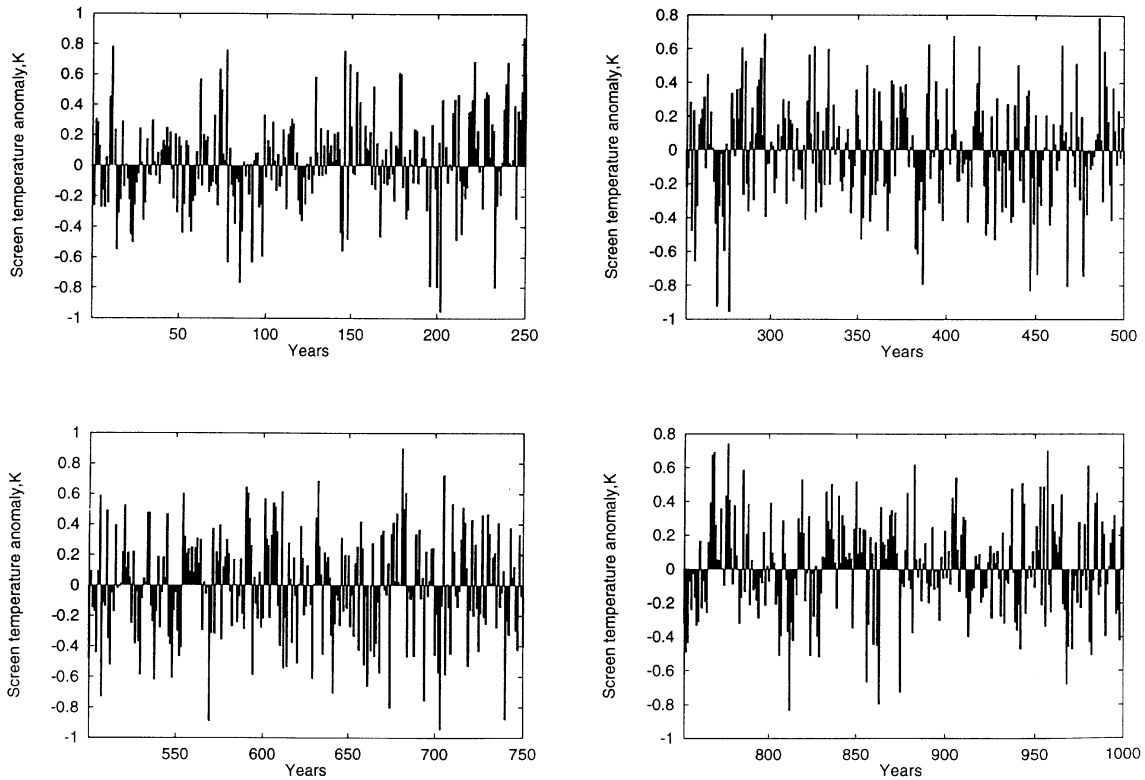


Figure 27 Histograms of annual mean screen temperature anomalies from the 1000-year simulation for the same model grid box in SWWA as used in Figure 26.

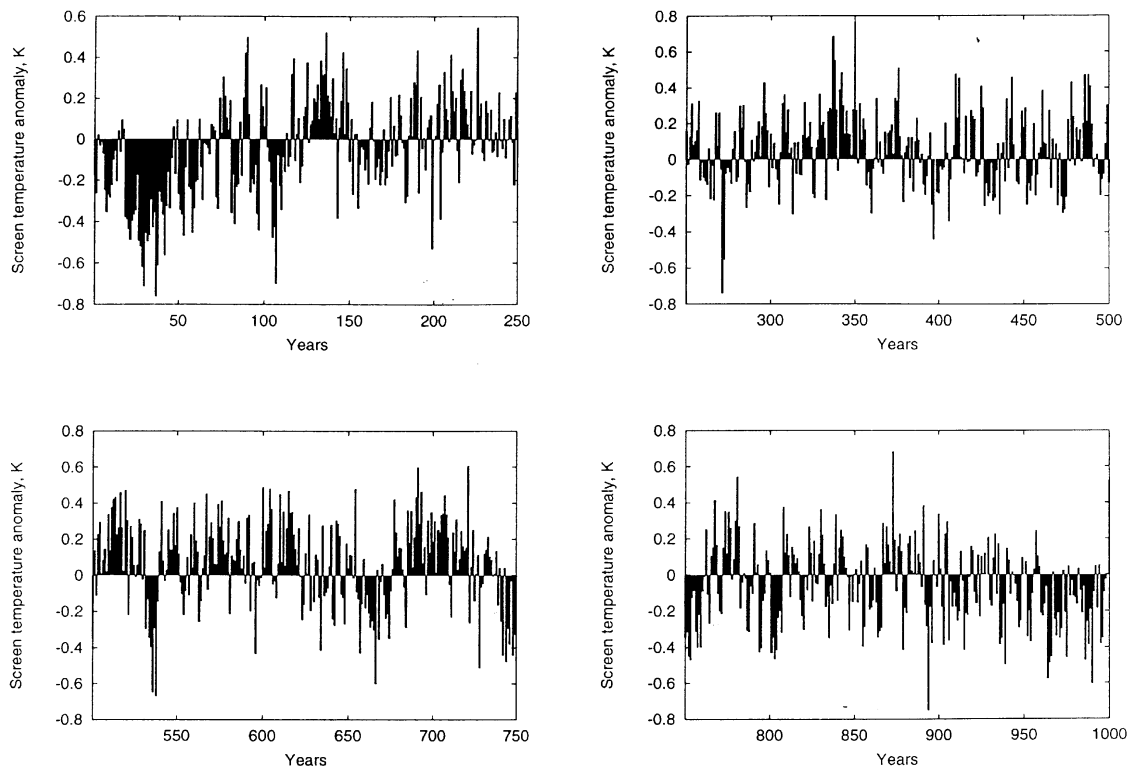


Figure 28 Histograms of annual mean screen temperature anomalies from the 1000-year simulation for a model grid box in the south Pacific Ocean, 220°E, 40°S.

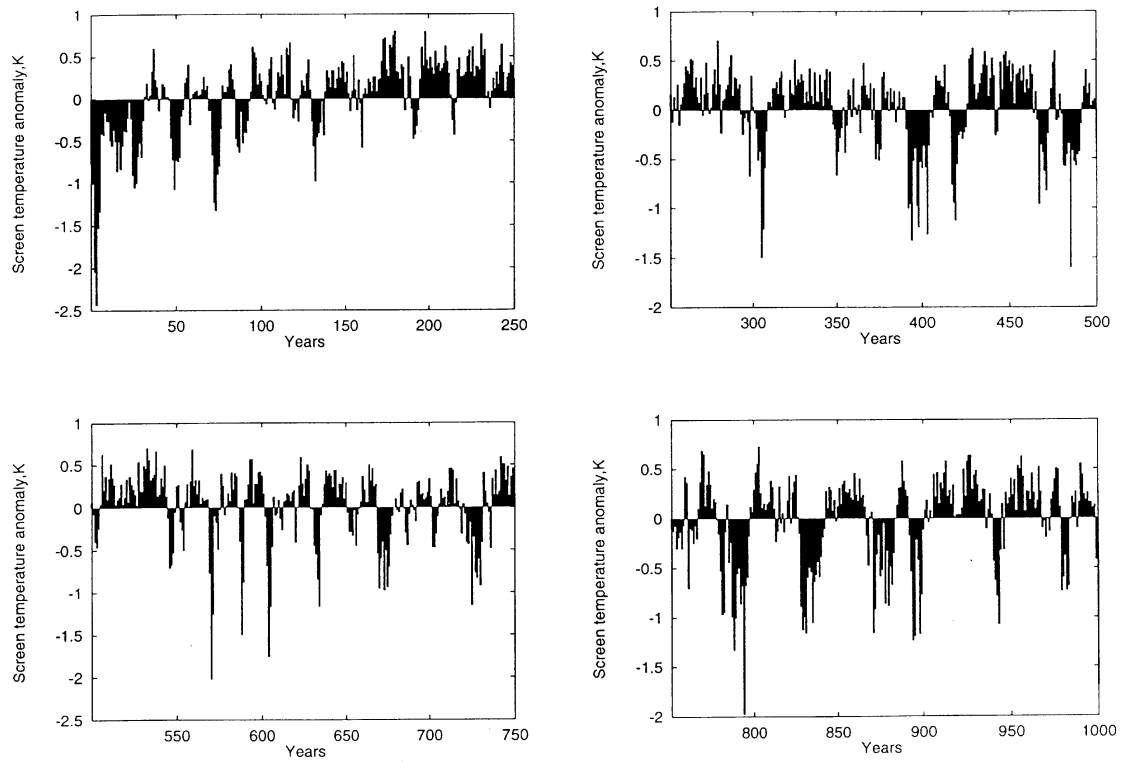


Figure 29 Histograms of screen temperature anomalies from the 1000-year simulation for a model grid box in the Southern Ocean, 130°E, 55.7°S.

The anomalous SST discussed above are not a simple artefact of the model. Figure 30 illustrates SST anomalies for two oceanic regions based on observations from the GISST data compilation. While only limited time series are available, Figure 30(a) shows that an approximate 40-year cooling trend occurred in the north-west Pacific earlier this century with SST anomalies of similar magnitude to those in Figure 28.

An examination was also made of oceanic temperatures. Figure 31 compares global distributions of oceanic temperature anomalies for a selected year for several oceanic depths. The large-scale anomalies shown in this figure can be identified at oceanic depths of several hundred metres indicating that the anomalies extend throughout the mixed layer region. An enormous amount of thermal energy is associated with such anomalies, which is why they persist for decadal or longer periods. Global plots of correlations between layer 1 and layer 4 (117 m) of the oceanic temperature anomalies reveal values of 0.4 to 0.8 over most of the oceans. Small or negative values occur north of Australia and into the Indian Ocean and also south of Africa. Such areas become larger as deeper layers are correlated with layer 1. A further indication of the correlation of the oceanic temperature anomalies of the various layers in the oceanic model is given in Figure 32, in which time series of oceanic temperature anomalies and the screen temperature for a selected grid box are compared for the 1000 years of the run. The same gross features can be seen at all four levels in the figure, with similar amplitudes and temporal variabilities. The shorter-term temporal variability tends to decline with depth, resulting in multi-annual features becoming more prevalent. At other grid boxes, variants of this behaviour occurred, but the largest differences were obtained in the tropics, where multi-annual ENSO events dominated at the surface. Owing to the relative shallowness of the mixed layer in this region, a quite different, multi-century variability was found at greater depths where layers below the thermocline were sampled.

Given the magnitude, depth penetration and persistence of these oceanic temperature anomalies, as shown in Figure 32, long-term impacts on other climatic variables can be expected. Exactly how ocean temperature anomalies at any one region create the climatic trends illustrated in the above figures, given all the other competing influences from other regions, is unknown. In particular, the manner in which such oceanic trends are related to rainfall variations over SWWA needs to be the subject of future research. At this stage, possible precursors for such rainfall variations have been identified.

The 1000-year simulation was also used to investigate a number of climatic features specific to SWWA.

Figure 33 shows annual mean rainfall anomalies for the Australian region for a sequence of 8 years where dry conditions prevailed over SWWA. Contrary to expectations, no systematic, synoptic system prevailed during this period. For example, while year 815 was associated with a large-scale rainfall anomaly over Western Australia, in year 816 the dry anomaly was isolated to SWWA alone. The following four years, 817-820, all had large-scale rainfall anomalies, but the remaining two years, 821-822, again had dry anomalies restricted to SWWA. These results are consistent with the multi-box correlations given above, in which the 1000-year correlation between 1 and 25 model grid boxes was quoted as 0.66. If the rainfall anomaly patterns in Figure 33 are representative of actual conditions over SWWA, they illustrate how difficult it is to establish cause-and-effect relationships for this region.

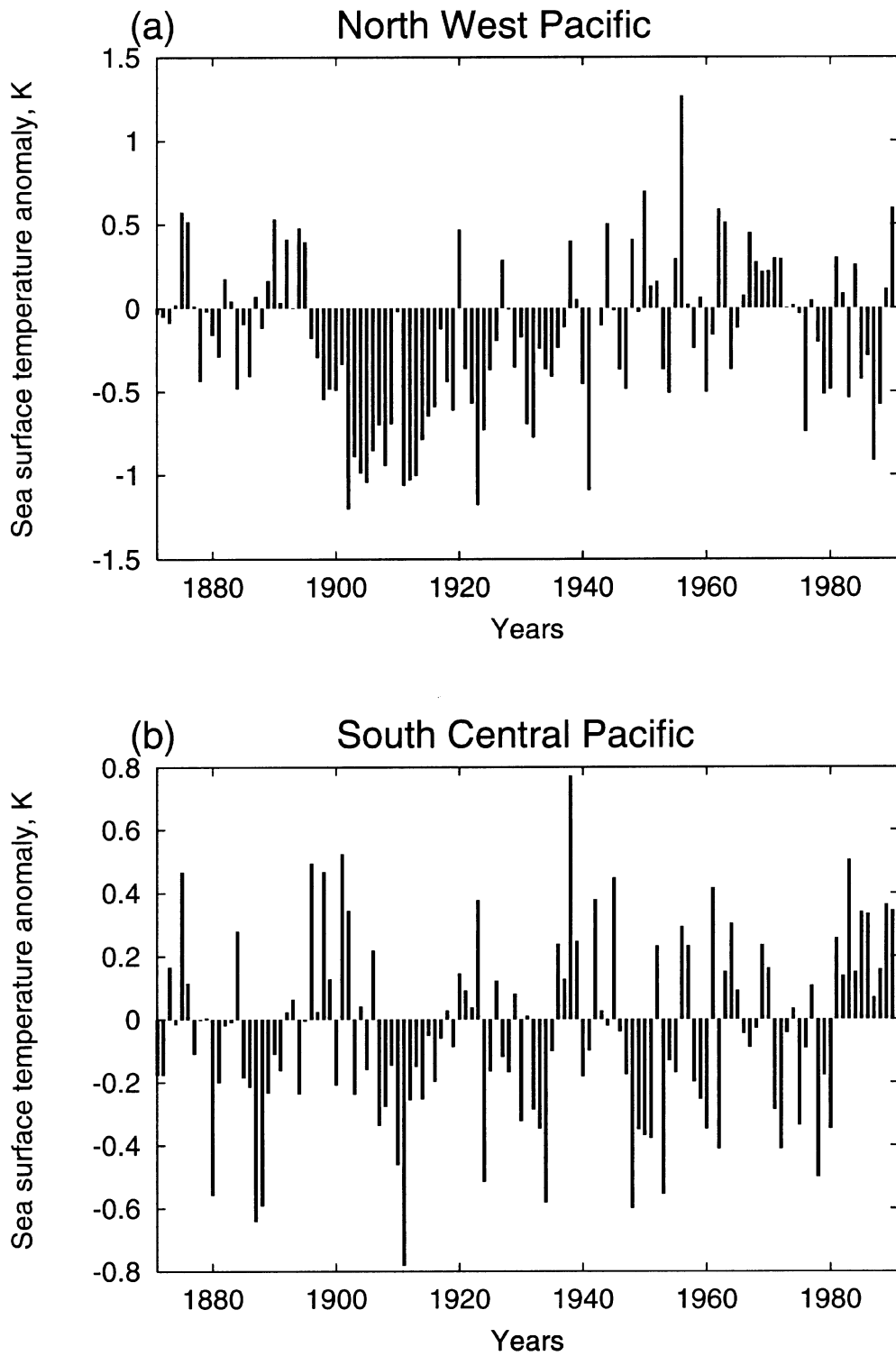


Figure 30 Observed sea surface temperature anomalies from the GISST data set. Results for the northwest Pacific Ocean (170°E, 45°N) are shown in the upper panel, and for the south central Pacific Ocean (220°E, 40°S) in the lower panel.

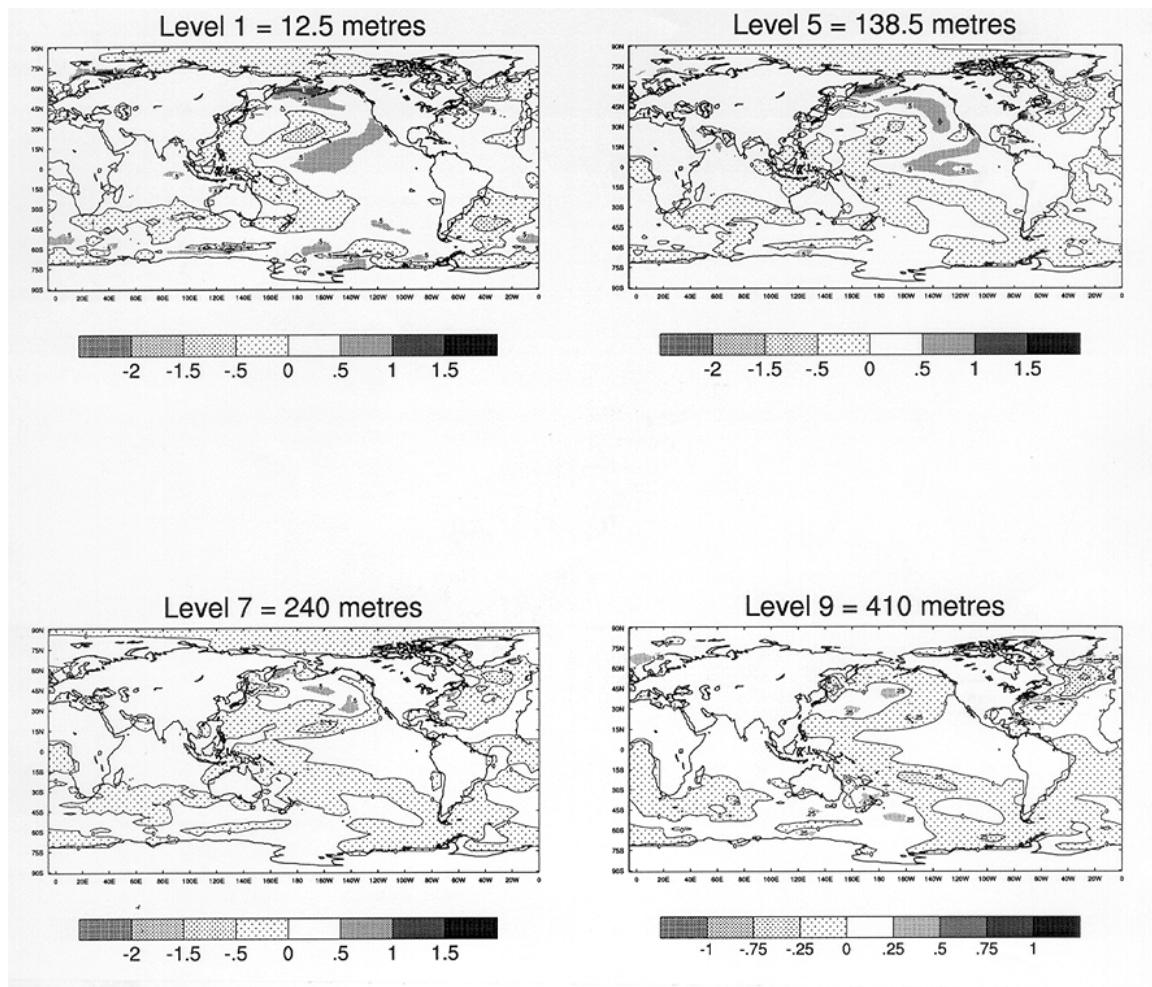


Figure 31 Oceanic temperature anomalies at various depths for a given year of the 1000-year simulation. The colour code identifier under the various plots is in °K.

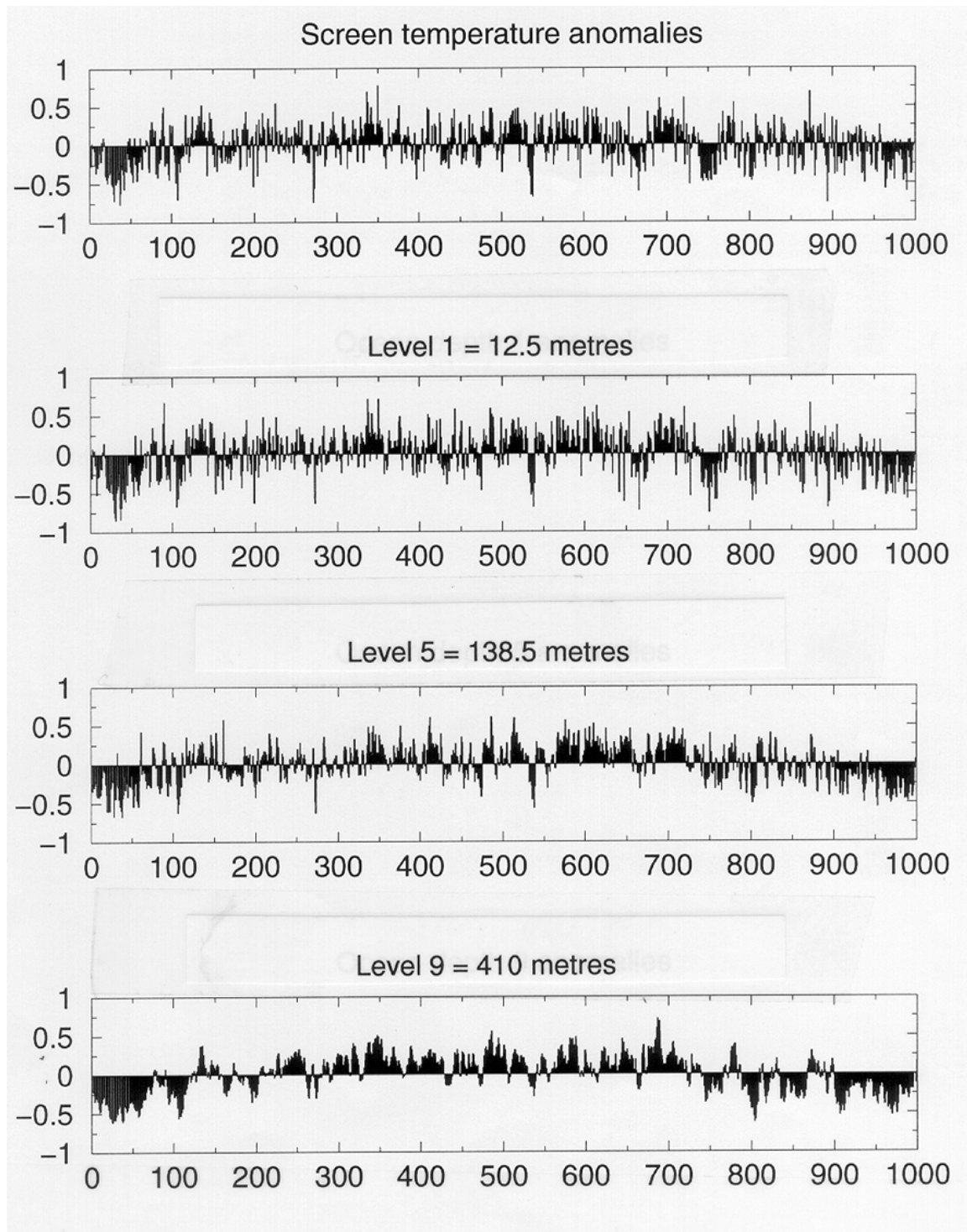


Figure 32 Histograms of screen temperature and ocean temperature anomalies from the 1000-year simulation for the same model grid box as used in Figure 28 (i.e. South Pacific Ocean, 220°E, 40°S).

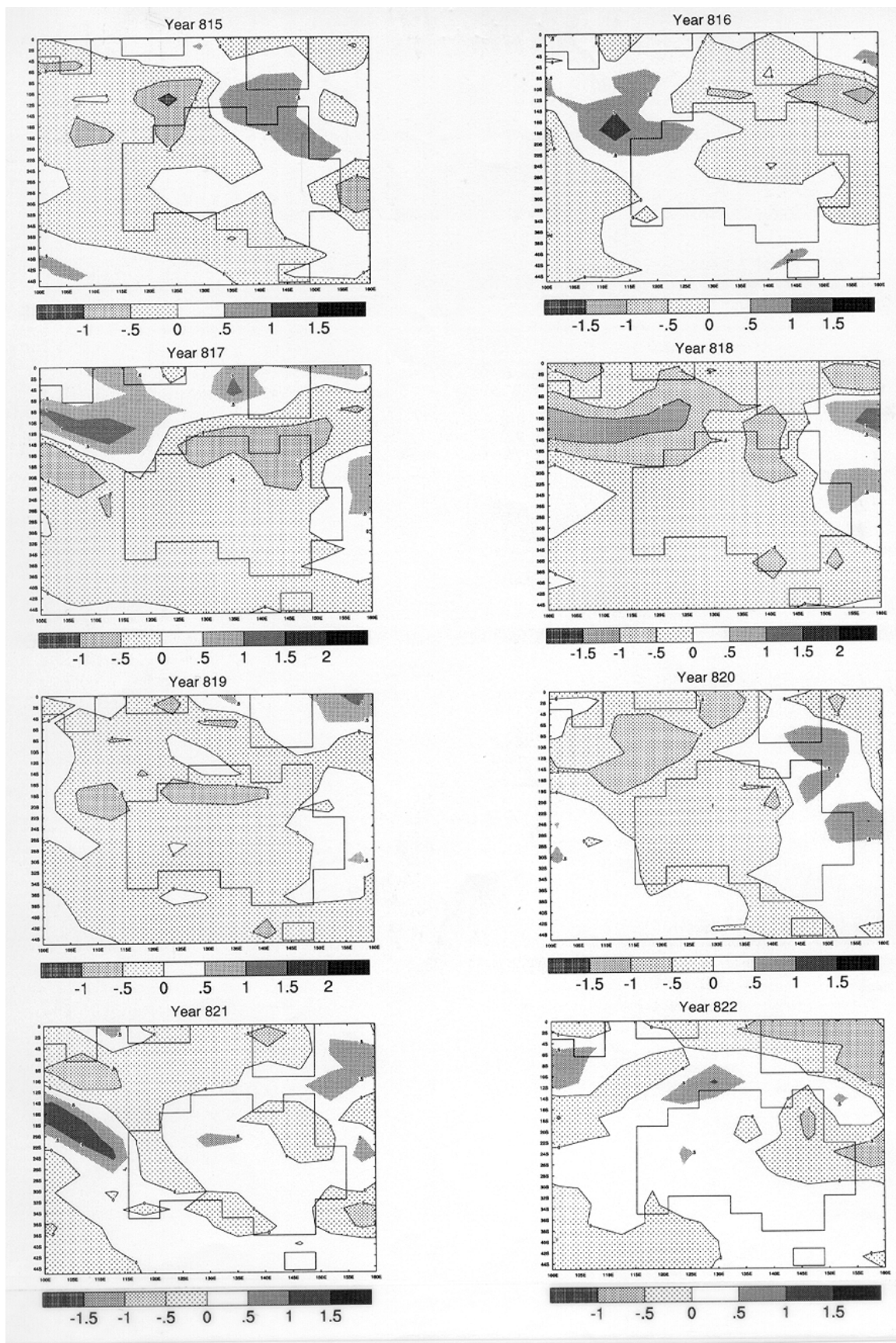


Figure 33 A sequence of rainfall anomalies from the 1000-year simulation associated with an eight-year drying trend in SWWA.

A series of one-point correlation maps were made from the 1000-year simulation for different climatic variables. These maps correlated the global distribution of the given variable with its value in SWWA, and provided an indication of the regions that interact with SWWA. For example, Figure 34 shows a one-point correlation map for screen temperature. This reveals that for correlation coefficients greater than 0.4, the major zones of interaction are over the Australian continent, extending into the Southern Ocean and also north-west into the Indian Ocean. A similar pattern was found for mean sea-level pressure, with no signal apparent over the Pacific Ocean.

In the case of rainfall, the spatial scale of the correlation pattern was much reduced in extent, with the major area of correlation again extending to the north-west and south-east. These results suggest that SWWA is rather isolated climatologically, with linkages to the north-west extending over the Indian Ocean and very little influence from the Pacific Ocean.

Finally, Figure 35 shows winter rainfall variability over SWWA from a simulation of the CSIRO Mark 2 coupled model, in which the effective carbon dioxide content of the atmosphere was allowed to increase to three times its present levels by the year 2083 and was then stabilised at this value. The figure reveals much interannual variability but with an underlying drying trend over the period to 2100 in which the carbon dioxide concentration was increasing. After concentration stabilisation, the rainfall recovers to its pre-greenhouse value.

Since the rainfall in Figure 35 decreases continuously from the year 1900, this suggests that, while greenhouse changes may influence rainfall in SWWA, they are not the sole cause of the major decline since the 1960s. Nevertheless, the potential influence of greenhouse-included climatic change is a question that should be considered in future research.

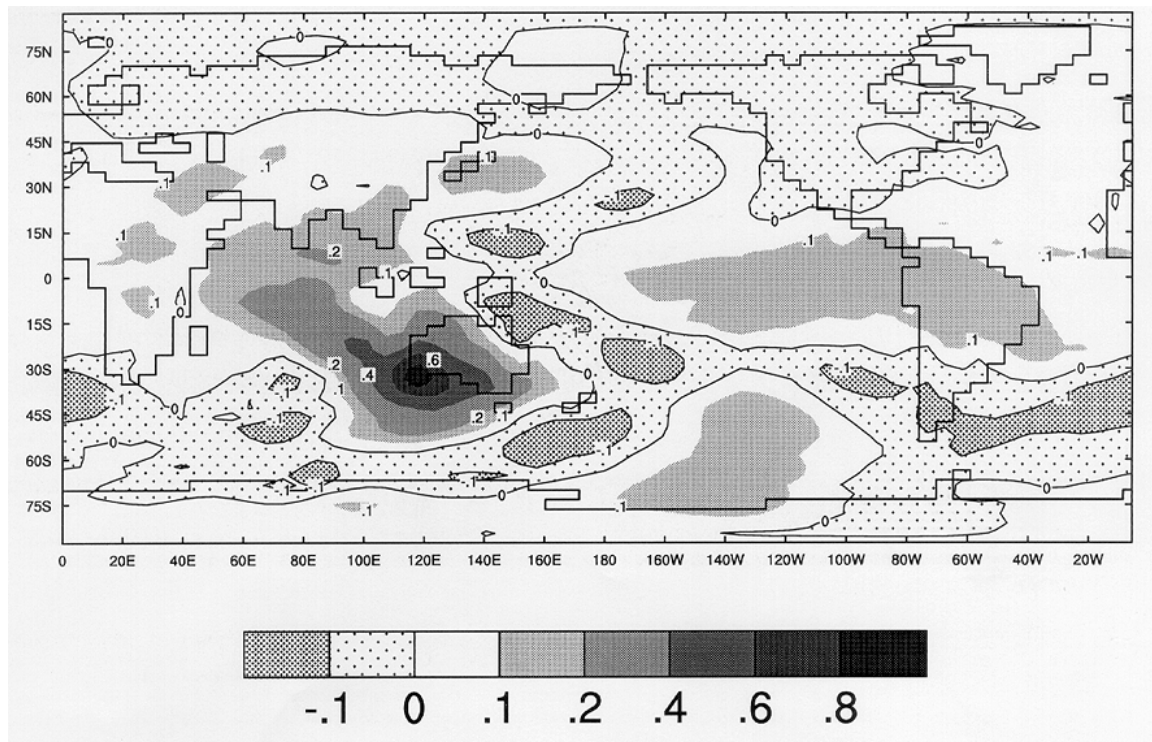


Figure 34 One-point correlation map for SWWA for screen temperature from the 1000-year simulation.

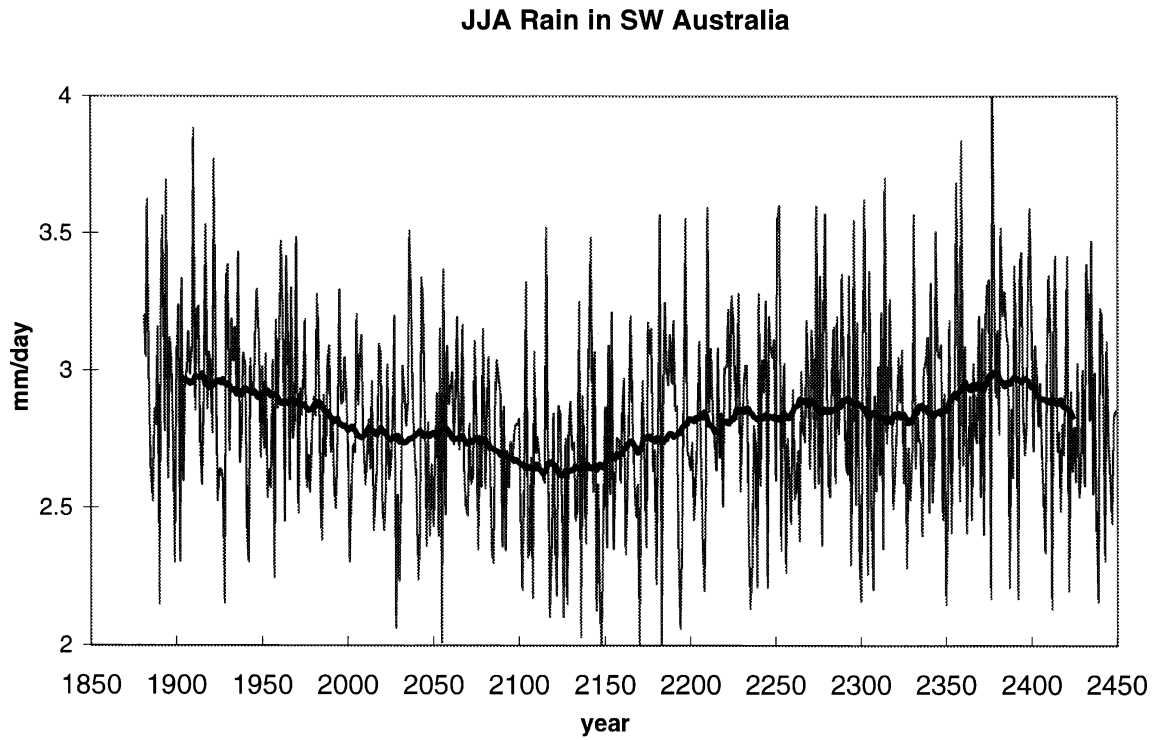


Figure 35 Simulated annual mean rainfall changes over SWWA under greenhouse conditions. The effective CO₂ content of the atmosphere was tripled between 1881 and 2083 AD and held constant thereafter. The thin line represents annual mean values for individual years, the thick line is a time-smoothed version of that curve.

CONCLUDING REMARKS

All of the objectives listed at the beginning of this report have been met and the outcomes achieved. Since this is the first year of a planned five-year research project, much of the research reported here has been of a scoping nature.

Thus, it has been demonstrated that synoptic systems relevant to SWWA can be adequately simulated with the CSIRO Mark 2 atmospheric global climate model.

The role of low-level winds over the Indian Ocean has been explored, and wind anomalies specifically associated with Pacific Ocean SST anomalies have been presented.

Importantly, it now appears from the 1000-year simulation with the CSIRO Mark 2 coupled model that previously established relationships between Indian Ocean SST dipole patterns, north-west cloud bands and rainfall anomalies are both driven by wind anomalies emanating from the subtropical Indian Ocean. The Indian Ocean dipole pattern does not appear to represent an independent source of variability.

Multi-seasonal predictions of SWWA rainfall using the existing CSIRO Mark 2 model and observed SSTs did not adequately capture the observed interannual variability. Improved SST data, particularly anomalies associated with the Antarctic Circumpolar Wave, may be required in order to improve this situation.

The interactions of multiple multi-annual to decadal climatic time variations, noted in observed data, further compound secular aspects of multi-seasonal predictions.

While the role of the north-west cloud bands in SWWA rainfall appears to be limited, there is a predictability signal associated with processes in the southern Indian Ocean. If these processes can be replicated in models then multi-seasonal predictions over SWWA may show improved skill.

An extensive study of climatic trends globally, and specifically over SWWA, has been undertaken using output from a 1000-year simulation from the Mark 2 CSIRO coupled model. This showed that extended, decadal or longer, climatic trends are a standard feature of climatic variability in many regions of the globe. Amongst the climatic variables considered, such trends were found to be shortest for rainfall and longest for screen

temperatures. In most places, a return period of about one 10-year “hard” trend per 1000 years was found for rainfall. Rainfall trends were found to be correlated over areas typical of synoptic systems, indicating organised physical processes are involved.

Given the role of SST anomalies in exciting climatic perturbations, these were also examined in the 1000-year simulation. The duration of trends, the regions influenced and the return periods for screen temperatures were found to be substantially more extensive than those for rainfall. Coherent temperature trends were found to exist throughout the depth of the mixed-layer ocean. Such temperature anomalies are associated with very large thermal inertias, hence the potential for such anomalies to perturb the climate.

The research reported here has identified and clarified many features associated with climatic trends over south-west Western Australia. Clearly, much remains to be done.

FUTURE RESEARCH OPTIONS

The following are some possibilities for the next phase of the Indian Ocean Climate Initiative Project, not all of which can be accomplished within one year.

Specific Projects

1. Modelling short-term variability

- Use the daily output from the 10,000-year run to investigate short-term rainfall variability and attempt to identify underlying climatic processes contributing to year-to-year variability.
- Systematically evaluate the 1000-year model output as regards the model’s ability to reproduce observed features such as El-Nino sea-surface temperatures patterns, the Indian Ocean dipole, Southern Ocean pressure patterns etc.

2. Seasonal and interannual timescales

- Use the Mark 3 T63 run, when completed, forced with observed sea-surface temperatures from 1871-1991 to explore possible relationships between sea-surface temperatures and south-west Western Australia rainfall.

- Evaluate multi-seasonal rainfall predictability with the Mark 2 and subsequently the Mark 3 prediction models.
3. *Decadal timescale*
- Examine the output from a recent greenhouse experiment using improved input fields (i.e. ozone and aerosols) for the period 1870-1990 to determine if a plausible signal exists regarding the south-west Western Australia drying trend.
 - Investigate whether the synoptic patterns over south-west Western Australia change during the 1870-1990 model run.
4. *Interdecadal variability*
- Composite warm and cold sea-surface temperature events in Indian and Southern Oceans and correlate separately with south-west Western Australia rainfall and highlight critical oceanic areas which are affecting this rainfall. This should identify oceanic regions which are important for predicting south-west Western Australia rainfall.
 - Use the global data set to expand the previous study to try to determine reasons for switches between trends of different sign. The daily data being generated in the 10,000 year run could also be used in this investigation.

REFERENCES

- Allan, R.J. (1999). ENSO and climatic variability in the last 150 years. Chapter 1 in Diaz, H.F. and Markgraf, V. (eds). *El Niño and the Southern Oscillation multiscale variability, global and regional impacts*. Cambridge University Press, Cambridge, U.K. (in press).
- Barnston, A.G., Glantz, M.H. and He, Y. (1999). Predictive skill of statistical and dynamical climate models in SST forecasts during the 1997-98 El Nino episode and the 1998 La Nina onset. *Bull. Amer. Met. Soc.*, 80(2), 217-249.
- Cai, W., Baines, P.G. and Gordon, H.B. (1999). Southern mid-to-high latitude variability, a zonal wavenumber 3 pattern, and the Antarctic Circumpolar Wave in the CSIRO coupled model. *J. Clim.* (accepted).
- Hunt, B.G. (1998). Natural climatic variability as an explanation for historical climatic fluctuations. *Clim. Change*, 38, 133-157.
- Hunt, B.G. (1999a). Natural climatic variability and Sahelian rainfall trends. Submitted to *Glob. Plan. Change*.
- Hunt, B.G. (1999b). Multi-seasonal hindcasts for 1972-1992. Submitted to *Month. Wea. Rev.*
- Nicholls, N. (1989). Sea surface temperatures and Australian winter rainfall. *J. Clim.*, 2, 965-973.
- Palmer, T.N. and Anderson, D.L.T. (1994). The prospects for seasonal forecasting – a review paper. *Quart. J.R. Met. Soc.*, 120, 755-794.
- Rowell, D.P. (1998). Assessing potential seasonal predictability with an ensemble of multidecadal GCM simulations. *J. Clim.*, 11, 109-120.
- Simmonds, I. and Trigg, G. (1988). Global circulation and precipitation changes induced by sea surface temperature anomalies to the north of Australia in a general circulation model. *Math. And Comp. In Simul.*, 30, 99-104.

- Smith, I.N., McIntosh, P., Ansell, T.J., Reason, C.J.C. and McInnes, K. (1999). South-west Western Australian winter rainfall and its association with Indian Ocean climate variability. *Int. J. Climatol.* (submitted).
- Stockdale, T.N., Anderson, D.L.T., Alves, J.O.S. and Balmaseda, M.A. (1998). Global seasonal rainfall forecasts using a coupled ocean-atmosphere model. *Nature*, 392, 370-373.
- Stone, R.C., Hammer, G.L. and Marcussen, T. (1996). Prediction of global rainfall probabilities using phases of the Southern Oscillation Index. *Nature*, 384, 252-255.
- Suppiah, R., Hennessy, K., Hirst, T., Jones, R., Katzfey, J., Pittock, B., Walsh, K., Whetton, P. and Wilson, S. (1998). Climate change under enhanced greenhouse conditions in northern Australia. Final Report 1994-1997 to Department of Lands, Planning and Environment, Northern Territory, Department of Environmental Protection, Western Australia and Department of Primary Industries, Queensland. CSIRO Division of Atmospheric Research, Aspendale, 50pp.